Chapter 4: Non-Linear Conservation Laws; the Scalar Case

4.1) Introduction

In the previous chapter we developed an understanding of monotonicity preserving advection schemes and Riemann solvers for linear hyperbolic systems. We saw that they are two of the essential building blocks that are used in designing schemes for linear hyperbolic systems. In this chapter we begin a study of non-linear conservation laws. Several of the hyperbolic systems of interest to us, such as the Euler equations, have strongly non-linear terms and can in fact be written in conservation form. Solutions for all these hyperbolic systems will, therefore, also be based on our twin building blocks of TVD limiting and Riemann solvers. However, the way these are implemented changes as we face up to the presence of non-linearities. This change is occasioned by the fact that the non-linear terms in a hyperbolic system can result in the formation of shocks and rarefactions. In our study of the Euler equations in Chapter 1, we alluded to these two flow structures, but we have not yet studied them in detail. It turns out that these interesting flow features find their analogues in the simplest of scalar, non-linear conservation laws. Furthermore, when seen in this simple context, they can be easily understood. For that reason, we focus on scalar conservation laws that have non-linearities in this chapter. We will study the formation of shocks and rarefactions for this simple system as a way of improving our intuition. We will see how the Riemann problem gets modified in the presence of non-linearities. All these insights will then be applied to the actual systems of interest in subsequent chapters.

We begin by considering the scalar, hyperbolic conservation law of the form

$$\mathrm{u}_t + \mathrm{f}\left(\mathrm{u}\right)_x = 0 \tag{4.1}$$

The conservation law in eqn. (4.1) will be hyperbolic if its eigenvalue $\mathrm{f}'\left(\mathrm{u}\right) \equiv \mathrm{df}\left(\mathrm{u}\right)/\mathrm{du}$ is real, a condition that is easily satisfied. A good way of deriving a conservation law of

this form would be to focus on the x-directional variations of the x-momentum equation in the Euler system and consider a situation where the pressure terms are negligible compared to the convective terms. The x-momentum then satisfies the form given in eqn. (4.1) with $f(u) = u^2/2$. This choice of flux yields an equation called the Burgers equation. It is easy to see that the Burgers equation is a non-linear, hyperbolic equation in conservation form. The Burgers equation has been thoroughly studied in the literature because it can produce most of the prototypical shock and rarefaction structures that we wish to study in subsequent chapters for systems of hyperbolic conservation laws.

Considerable conceptual simplification results if the flux is also *convex*, i.e. if $f''(u) \equiv d^2 f(u)/du^2$ does not change sign. The sign of $f''(u)$ can be positive or negative. Physically, it means that the speed, $f'(u)$, monotonically increases or decreases with increasing "u". For example, it is easy to see that the Burgers equation is convex. Similarly, it can be shown that the flux for the Euler equations is also convex in a special way that is as yet undefined for hyperbolic systems. Convexity, along with strict hyperbolicity confers an important physical simplification to the hyperbolic system because it ensures that shocks and rarefactions of a given characteristic family remain disjoint from similar structures from another characteristic family. This enables one to prove that certain solution techniques for a hyperbolic system with a convex flux will produce results that will always converge to the physical solution (Lax 1972, Harten 1983a). We, therefore, devote much of our attention in this chapter to scalar hyperbolic equations with convex fluxes. We do, however, point out that many physical systems can be *non-convex*, prominent examples being the MHD and non-linear elasticity systems. The mathematically rigorous demonstration that general solution techniques exist for non-convex hyperbolic systems has not advanced as far as one would like (Oleinik 1957, 1964, Isaacson & Temple 1986, Isaacson, Plohr & Temple 1988, Keyfitz 1986, Keyfitz & Mora 2000, Schaeffer & Shearer 1987a,b, LeFloch 2002). While we will not discuss non-convex conservation laws in any great detail in this chapter, some of the boxes at the ends of the sections provide comparisons between convex and non-convex scalar, hyperbolic equations.

Section 4.2 gives us a very gentle and intuitive introduction to shock and rarefaction waves. Section 4.3 is a more detailed study of isolated shock waves. Section 4.4 studies rarefaction fans in further detail. Section 4.5 shows how shock wave and rarefaction fans can be used in the design of Riemann solvers. Section 4.6 discusses boundary conditions. Section 4.7 provides a couple of numerical methods for the solution of scalar hyperbolic conservation laws.

4.2) A Gentle Introduction to Rarefaction Waves and Shocks

Before we develop a sophisticated understanding of rarefaction waves and shocks, it helps to develop our intuition by considering a simple mechanistic model. Such an intuitive model will help us a lot as we study rarefactions and shocks further in subsequent sections. We build such a mechanistic model for rarefaction waves first and then do the same for shocks in Sub-Section 4.2.1. In Sub-Section 4.2.2 we show how shocks and rarefactions form in a non-linear hyperbolic equation. Sub-Section 4.2.3 reinforces these concepts by showing that similar shock and rarefaction wave solutions occur naturally when considering the simplest form of a scalar, non-linear hyperbolic problem, i.e. the Burgers equation. Sub-Section 4.2.4 discusses simple wave solutions of the Burgers equation.

4.2.1) A Mechanistic Model for Rarefaction Waves and Shocks

Consider a model for rarefaction fans that is based on skiers skiing downhill. Fig. 4.1 provides a schematic diagram. At the top of the hill we have a number density n_0 of skiers all of whom are bunched up as tightly as possible in a row. (The density in this sub-section refers to the number of skiers per unit length, i.e. it is a linear density.) The row of skiers moves with a speed v_0 to the top of the ski ramp. We then have a flux of skiers given by $n_0 v_0$ who are entering the ski ramp. As the skiers go downhill, the frictional forces are minimal to begin with so that the velocity $v(x)$ as a function of "x"

from the top of the hill is given by $v^2(x) = v_0^2 + 2\,g\,x\sin\theta$. At a distance "*x*" let the number density of skiers be $n(x)$. Flux conservation then gives us $n_0\,v_0 = n(x)\,v(x)$. We can therefore obtain the number density of skiers at any distance "*x*" as $n(x) = n_0\,v_0 \Big/ \sqrt{v_0^2 + 2\,g\,x\sin\theta}$. The inset plot shows the variation of $n(x)$ and $v(x)$ as a function of "*x*". We see that the number density of skiers decreases as the skiers pick up speed. In other words, there is a *rarefaction wave* associated with the skiers as they go downhill. Notice that the skiers that make up this rarefaction wave keep changing, however, the shape of the rarefaction is preserved. In time we will see, quite analogously, that the atoms that make up a hydrodynamical rarefaction wave also keep changing and yet the shape of the rarefaction wave can be preserved in certain situations. Notice too that we were able to derive our result purely from considerations of conservation and an assertion that the flux of skiers needs to be preserved at each location down the hill. We will soon learn that the structure of a rarefaction wave is determined by the form of the flux in the conservation law.

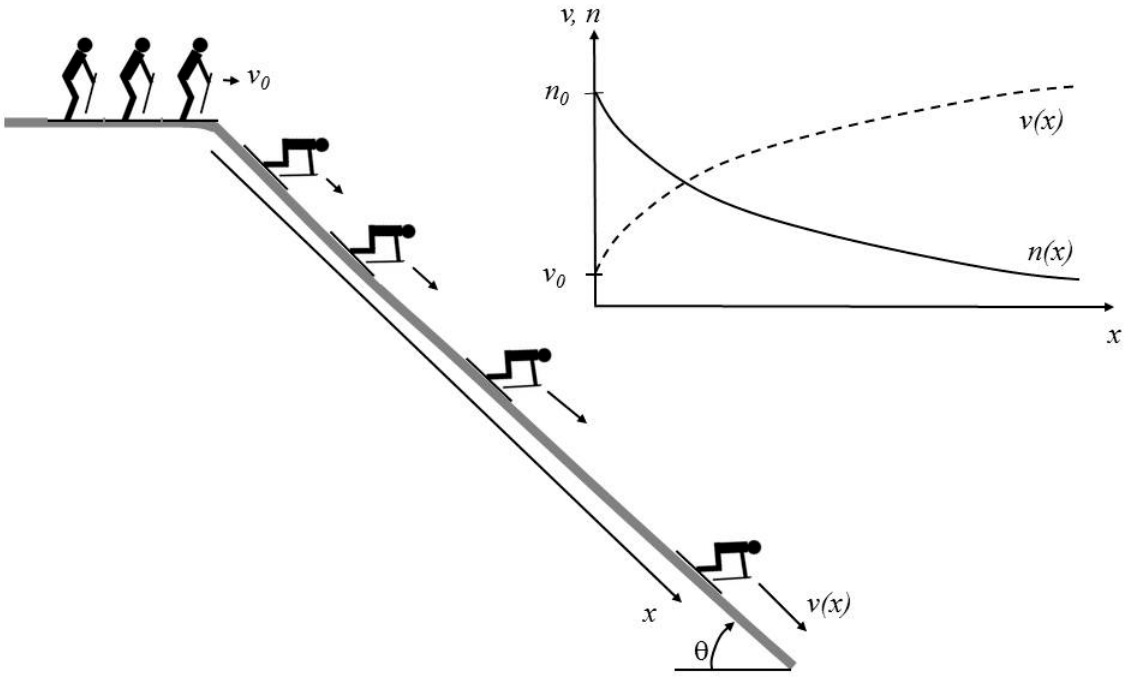

Fig. 4.1 shows how a rarefaction wave may form among skiers taking off from a hill. As the skiers pick up speed downhill, their density decreases. The rarefaction wave is not made up of any set of skiers; instead, individual skiers flow through the rarefaction. The inset plot shows the variation of the density of skiers (solid line) and their velocity (dashed line) as a function of distance "x" from the top of the hill. Notice that the density of skiers decreases, i.e. rarefies with "x".

We can also make a simple model for *shock waves* by extending our analogy to the skiers going downhill. Say that there is a tree close to the bottom of the hill as shown in Fig. 3.2. The first skier comes down fast enough with the result that he cannot reduce his speed in time and, therefore, collides with the tree. The skiers that follow him are similarly unfortunate and begin piling up one behind the other via a sequence of collisions. At the scene of the pile-up, the skiers are again as closely packed as they were at the top of the hill, so that their density is given by n_0. The point where the collision happens begins to move to the left with a negative speed "*s*". We call this speed the *shock speed*. Let the number density of skiers at the bottom of the hill before the collision be given by n_b and let their velocity before collision be given by a positive number v_b. We can again apply flux balance to this situation. Say we do it in a coordinate frame that moves with the shock. The speed of the skiers coming into the shock from the left, as measured in the shock's rest frame, is $(v_b - s)$ so that the flux of skiers coming into the

shock from the left is given by $n_b\left(v_b - s\right)$. The flux of skiers leaving the shock to its right, again measured in the shock's rest frame, is given by $-n_0\ s$. Balancing the fluxes on either side of the shock then gives us $n_b\left(v_b - s\right) = -n_0\ s$. Notice that as the pile-up proceeds, the shock moves to the left so that we expect the shock speed to be negative. Using the above equation for flux balance we can now write the shock speed as $s = -\ n_b\ v_b / \left(n_0 - n_b\right)$. As with rarefaction waves, notice that all we had to do was rely on a conservation law to derive the shock speed, i.e. all we had to do was conserve the number of skiers. This was done by applying a principle of detailed balance to the flux of skiers.

Notice that the location of the shock wave is not demarcated by any single skier; rather, the shock front sweeps over the skiers as they enter it from the left in Fig. 4.2. In an analogous fashion, the atoms that enter a hydrodynamical shock do not demarcate the location of the shock as they enter it from one side. Instead, the shock wave overruns the atoms as they keep entering it. Just as the density of skiers can change as they enter a shock, the density of gas molecules entering a shock can also change by a considerable amount. The fluid fluxes measure the rate at which atoms enter a hydrodynamical shock as well as the rate at which momentum and energy are carried into the shock by those atoms. We will soon learn that the structure of a shock wave is determined by the form of the flux in the conservation law. In our simple example with skiers, we saw that the flux of skiers entering and leaving the shock have to be balanced in the shock's own rest frame. In time we will see that the fluxes of mass momentum and energy also have to be balanced in the rest frame of a hydrodynamical shock.

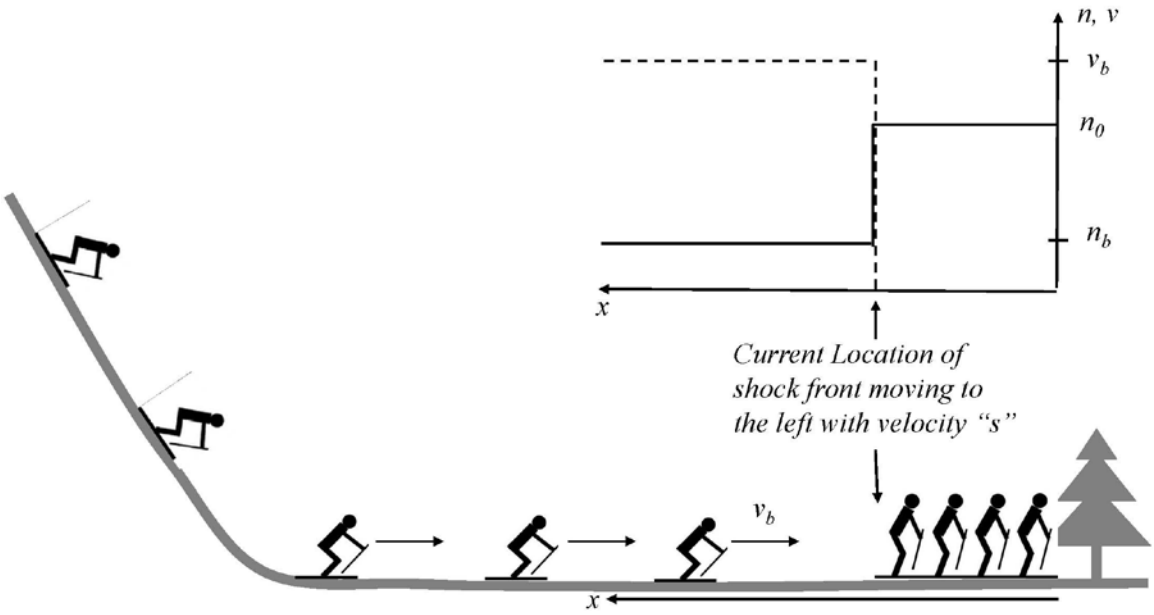

Fig. 4.2 depicts how a shock wave might form among skiers who ski down a hill and pile up against each other due to an initial collision with a tree. The shock front moves leftward with velocity "s" as each successive skier collides with the one before him. The density of skiers is lower in front of the shock and higher behind the shock. The speed at which the shock front propagates is related to the flux of skiers coming into the collision. However, the shock front is not demarcated by any one skier. The inset plot on top shows the density of skiers (solid line) and velocity of skiers (dashed line) as a function of position "x" from the tree.

4.2.2) The Formation of Shocks and Rarefaction Waves

Let us study the shocks and rarefaction waves produced by the Burgers equation given by

$$u_t + \left(\frac{u^2}{2} \right)_x = 0 \qquad (4.2)$$

The equation can also be written in the non-conservative form

$$u_t + u\, u_x = 0 \qquad (4.3)$$

Eqn. (4.3) shows us that the characteristics of the equation still propagate in space-time with a speed "u"; however, "u" is no more a constant as it was for the scalar advection

case. Thus if we consider a smooth and differentiable initial condition $u_0(x)$ for all points along the *x*-axis, we can formally write the solution for all later times as

$$u(x,t) = u_0(x_0) \qquad \text{where} \quad x_0 = x - f'(u_0(x_0))t \tag{4.4}$$

where $f'(u) \equiv d\,f(u)/d\,u$. Fig. 4.3 illustrates the analytic solution strategy that is catalogued in eqn. (4.4). We see that x_0 is the foot point of the characteristic $x = x_0 + f'(u_0(x_0))t$ on the x-axis. If we know the value of the solution $u_0(x_0)$, we can find the characteristic's speed of propagation, $f'(u_0(x_0))$. We then see that the solution $u(x,t)$ at a later time is simply given by following the characteristics backward in time to the initial condition $u_0(x_0)$. We shall soon see, however, that x_0 is not always easy to find. Compare eqn. (4.4) to the advection equation, $u_t + a\,u_x = 0$, which for the same initial conditions gives us the solution $u(x,t) = u_0(x - a\,t)$. Both equations tell us that the solution at any position *x* and any time $t > 0$ is obtained by following the characteristic that passes through (x,t) back to its starting position on the *x*-axis. Figs. 2.13 and 4.3 illustrate the similarities as well as the differences. We see that in both cases we follow the characteristic reaching the space-time point (x,t) back to its foot point x_0 on the *x*-axis and read off the value $u_0(x_0)$ to obtain the solution. The difference, however, stems from the fact that the characteristics in Fig. 4.3 are not parallel lines but instead depend on the solution. Thus obtaining the foot point x_0 would entail solving the transcendental equation $x_0 = x - f'(u_0(x_0))t$ in eqn. (4.4). Unless $f'(u)$ and $u_0(x_0)$ have very simple analytical forms, solving the transcendental equation can be quite difficult. In contrast, the characteristics in Fig. 2.13 are all parallel straight lines with the result that obtaining the foot point $x_0 = x - a\,t$ on the x-axis for the scalar advection equation is always easy.

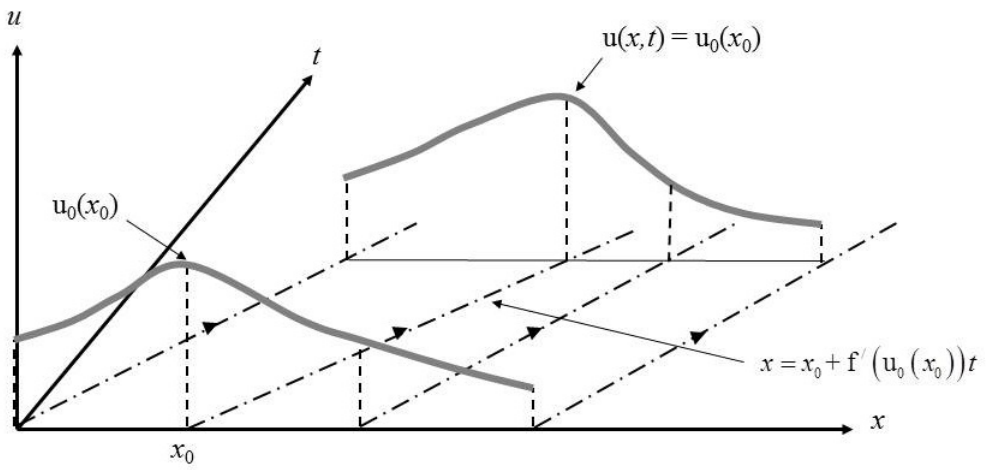

Fig. 4.3 showing the time-evolution of the Burgers equation $u_t + (u^2/2)_x = 0$.
Think of it as a three-dimensional figure where the height above the x-t plane shows the solution. The dot-dash lines with arrows show the characteristics in the x-t plane. The thick grey curves represent the solution "$u_0(x)$*" at time t=0 and its evolution in time, "*$u(x,t)$*".*

Notice from Fig. 4.3 for the Burgers equation that the characteristic speeds are equal to the value of the solution "u". As a result, those characteristics that correspond to the rightward face of the profile shown in Fig. 4.3, are converging with time while those corresponding to the leftward face diverge as time progresses. Converging characteristics cause the solution to steepen; diverging characteristics cause the slope of the solution to decrease with time. This results in a steepening of the rightward face and a loss in steepness at the leftward face, as can be observed from Fig. 4.3. If we extend the characteristics onward in time, we see that they will intersect for the part of the solution that has $\partial u(x,t)/\partial x < 0$. To find the point in time where two adjacent characteristics intersect, consider a point x_0 on the *x*-axis with $\partial u(x_0, t=0)/\partial x < 0$ and consider an adjacent point that also lies on the *x*-axis at $x_0 + \Delta x_0$ a very small distance away from the first point. The two characteristics emanating from these two adjacent points are given by

$$x = x_0 + f'(u_0(x_0))t \quad \text{and} \quad x = x_0 + \Delta x_0 + f'(u_0(x_0 + \Delta x_0))t \tag{4.5}$$

Since the two equations in eqn. (4.5) are straight lines in space-time, it is easy to find their point of intersection. We can then take the limit $\Delta x_0 \to 0$ to ensure that the two foot

points are truly adjacent. The characteristics intersect at a time $t = -1 \Big/ \left[\mathrm{f}'' \left(\mathrm{u}_0 \left(x_0 \right) \right) \mathrm{u}_0' \left(x_0 \right) \right]$. By letting x_0 range over the *x*-axis, we can now find the earliest time that any two adjacent characteristics will intersect. This is called the *breaking time*, in analogy with the process of seeing a water wave break. It is given by

$$T_{break} = \frac{-1}{\min_x \left[\mathrm{f}'' \left(\mathrm{u}_0 \left(x \right) \right) \mathrm{u}_0' \left(x \right) \right]} \tag{4.6}$$

We therefore see that the non-linearity of the Burgers equation causes the converging characteristics to intersect in a finite amount of time. This intersection is sure to happen for solutions of the Burgers equations provided the initial conditions have a negative gradient in the x-direction. Past the breaking time, if we simply allow the solution to propagate along characteristics then we see that the solution will become double valued in space – a situation which we would find totally unacceptable. The only resolution consists of accepting that a discontinuous solution develops at the breaking time and propagates with a certain speed. We call such a discontinuous solution a *shock* and we call the speed with which it propagates the *shock speed*. Sub-Section 3.4b has already shown us that hyperbolic systems can have discontinuous solutions. We will next take a specific profile, study its time evolution and indeed convince ourselves that discontinuous solutions do develop for the Burgers equation.

4.2.3) Shock and Rarefaction Wave Solutions Arising from the Burgers Equation

Consider the solution of the Burgers equation with the initial condition $\mathrm{u}_0 \left(x \right) = 0.5 + \exp\left(-100 \left(x + 0.25 \right)^2 \right)$. Fig. 4.4 shows the solution in the interval $\left[-0.5, 0.5 \right]$. The evolution of this profile at times $t = 0,\ 0.08,\ 0.1116$ and 0.6 is shown in Figs. 4.4a through 4.4d . The panel at the bottom of each of those figures displays a small space-time plot showing the evolution of the characteristics in space and time for 0.03 units of time after the time at which the solution is shown in each of those figures. These small panels, therefore, illustrate how the solution will evolve for a short interval of time

after the times shown. Since the characteristic speed is given by the solution “u” for Burgers equation, we see from Fig. 4.4a that the characteristics on the right face of the Gaussian point are converging into each other, therefore implying that the right face of the Gaussian will steepen as it evolves in time. The characteristics on the left face of the Gaussian diverge from each other, implying that the left face will spread out in time. Fig. 4.4b at a later time shows that the expectations that we had built up by examining the characteristics in Fig. 4.4a have indeed been borne out. Since the Burgers equation is non-linear, Fig. 4.4b shows that the characteristics from the right face have become even more convergent, while those from the left face have begun to diverge even further. We say that the right face of the profile shown in Fig. 4.4b is a *compressional wave* whereas the left face is a *rarefaction wave*. Eqn. (4.6) shows that the breaking time for the Burgers equation with our initial conditions is 0.1166. Thus we expect at least some of the characteristics to begin intersecting by this time. Fig. 4.4c shows the solution at a time of 0.1116 , i.e at the very moment when the characteristics should intersect. We see that the right face of the Gaussian has steepened up considerably while the left face has spread out substantially. The panel at the bottom of Fig. 4.4c shows that the characteristics have indeed begun to intersect, indicating that a shock has begun to form. In other words, Fig. 4.4c shows that the compressional wave from Fig. 4.4b has begun to turn into a *shock wave*. Fig. 4.4d shows the solution a long time after the shock has formed. We see that the right face of the initial Gaussian has turned into a discontinuous solution while the left face of the initial Gaussian has turned into a rarefaction wave. This is in fact a very general property of hyperbolic systems and it was shown by Chandrasekar (1943) that the long term evolution of such convex hyperbolic systems would be a solution that looks like the letter “N” (or a flipped version of “N”). In other words, the solution will have a shock at each of its two ends with a rarefaction in between. Fig. 4.4d shows some of the ingredients of an N-wave.

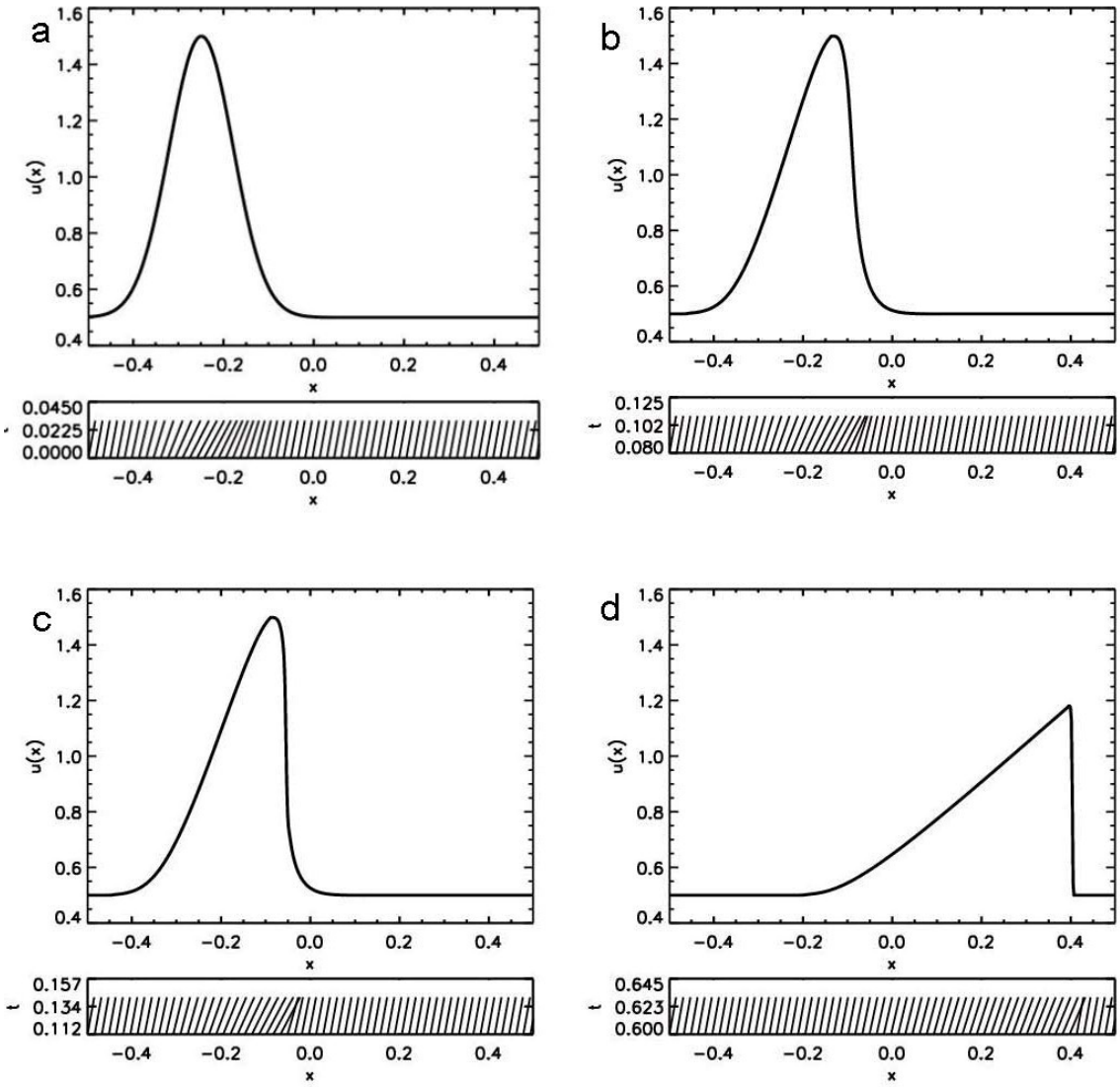

Figs. 4.4a to 4.4d show the solution of the Burgers equation with initial conditions given by the Gaussian pulse at times of 0, 0.08, 0.1116 and 0.6. The panel below each plot shows the time evolution of the characteristics for a short time interval, i.e. 0.03, after the time shown. Notice that the characteristics begin to intersect soon after a time of 0.1116, i.e. when the shock forms.

Fig. 4.4e shows the trajectories of the characteristics in space-time. It was obtained by initializing an evenly spaced set of tracer particles at $t = 0$ and evolving them in space-time with a speed given by the characteristic speed. Since the overall flow of characteristics is to the right, some more characteristics were allowed to enter the space-time domain from the left boundary. Fig. 4.4e clearly shows that the characteristics begin

to converge at the right face of the Gaussian and that they first begin to intersect at $t = 0.1166$. Once they begin to intersect, one can imagine the discontinuous solution for any time $t > 0.1166$ as representing the entire range of values of the characteristics that converge into it at that time. Thus we see that the locus of the shock in Fig. 4.4e is formed by the set of space-time points where the characteristics intersect.

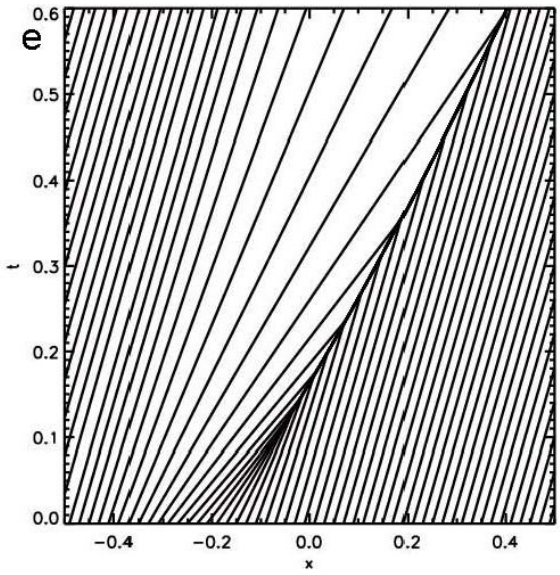

Fig. 4.4e shows the characteristics in space-time. The shock forms when the characteristics intersect. The position of the shock is shown by the thick line at which the characteristics intersect. We also observe that the characteristics diverge at the location of the rarefaction wave.

From an information theoretic viewpoint, we may even think of the characteristics as carrying information. Once those characteristics converge into a shock, the information disappears at that shock. Our invocation of ideas from information theory immediately reminds us of the second law of thermodynamics. In information theory, a loss of information is related to an increase in entropy. We realize that information may be lost at the location of the shock, but it can only be done at the expense of an increase in entropy. Indeed, if we think for a moment about a fluid dynamic shock, we realize this concept of entropy would coincide exactly with the physical entropy of the fluid. Based on our intuition we understand that when a strong fluid dynamical shock propagates through an object, thereby vaporizing it, the information contained in the molecular configuration of that object is indeed irreversibly obliterated. However, that loss of information comes with a corresponding increase in thermodynamic entropy. We, therefore, see that the ideas developed by studying shocks in Burgers equation have an exact correspondence with the fluid dynamical case. Indeed, Lax (1972) was able to show that one can define a concept of entropy for any scalar hyperbolic equation with a convex

flux function. Moreover, once characteristics flow into a shock, the information that they initially contained is irreversibly obliterated. In other words, different initial conditions can give rise to the same shock and we cannot use the structure of the shock at a later time to reconstruct all of the different types of initial conditions that could have given rise to it.

Fig. 4.4e shows us that the characteristics to the left of the shock begin to spread out as time evolves. By relating these characteristics at later times to Fig. 4.4d we realize that it forms a rarefaction wave. Fig. 4.4e has, therefore, provided us our fundamental insight that for a hyperbolic system with a convex flux the characteristics flow into a shock whereas they form diverging structures at a rarefaction wave. In the next sub-section we study idealized forms for shocks and rarefactions.

4.2.4) Simple Wave Solutions of the Burgers Equation

Sub-Section 3.4.2 has shown us that linear hyperbolic systems can also sustain discontinuous solutions. In this paragraph we study the evolution of the discontinuous initial conditions given by $u_0(x) = 2$ for $x < -0.25$ and $u_0(x) = 0$ for $x \geq -0.25$. Notice that the initial conditions are constant on either side of the initial discontinuity. Such constant conditions on either side of an initial discontinuity are sometimes referred to as the left and right states of the initial discontinuity. Observe too that the characteristic speeds to the left and right of the initial discontinuity are given by $f'(2) = 2$ and $f'(0) = 0$, i.e. the initial characteristics are flowing into the discontinuity. Fig. 4.5 shows the solution in the interval $[-0.5, 0.5]$. The evolution of this profile at times $t = 0,\ 0.3$ and 0.6 is shown in Figs. 4.5a through 4.5c . The panel at the bottom of each of those figures displays a small space-time plot showing the evolution of the characteristics in space-time for 0.01 units of time after the time at which the solution is shown in each of those figures. As in Fig. 4.4, these small panels, therefore, illustrate how the solution will evolve for a short interval of time after the times shown. From Fig. 4.5a we see that the characteristics intersect at $x = -0.25$ even at $t = 0$ so that the

discontinuity starts off as a shock. Fig. 4.5b shows us that the discontinuity has propagated in a form-preserving fashion to a location $x = 0.05$ by time $t = 0.3$. Fig. 4.5c shows us that the discontinuity propagates in a self-similar fashion to a location $x = 0.35$ by time $t = 0.6$. We deduce, therefore, that the discontinuity propagates with a unit speed. In the next section we will show that the speed of propagation of the discontinuity depends only on the values of the solution on the left and right of the discontinuity as well as on the form of the flux function. Such a self-similar discontinuity is sometimes referred to as an *isolated shock wave* and is analogous to the simple waves studied in Sub-Section 3.4.2. See eqns. (3.32) to (3.35) for a description of simple waves in linear hyperbolic systems.

Just as the self-similar propagation of simple waves in a linear hyperbolic system depends on the structure of the characteristic matrix, the propagation of isolated shocks depends on the structure of the flux function. However, the speed of propagation of a simple wave is independent of the jump in the solution across the discontinuity. In contrast, we will see that the speed at which an isolated shock propagates does depend on the values of the piecewise constant initial conditions on either side of it. This can be intuitively understood by examining the small panels at the bottom of Figs. 4.5a to 4.5c. The points where the characteristics intersect a time interval 0.005 after the times shown in those plots are indeed the points to which the shock will propagate in that time interval. The characteristics, therefore, give us a very mechanistic view of shock propagation. Fig. 4.5d shows us the characteristics in space-time. We clearly see that the shock is the locus of the intersection of the characteristics from the right and left of the discontinuity. Should the values of the initial conditions on either side of the discontinuity be altered, the propagation speeds of the characteristics would also be changed. This would alter the location at which the characteristics intersect and, therefore, change the speed of shock propagation. This is an important point of difference between linear hyperbolic systems and their non-linear counterparts.

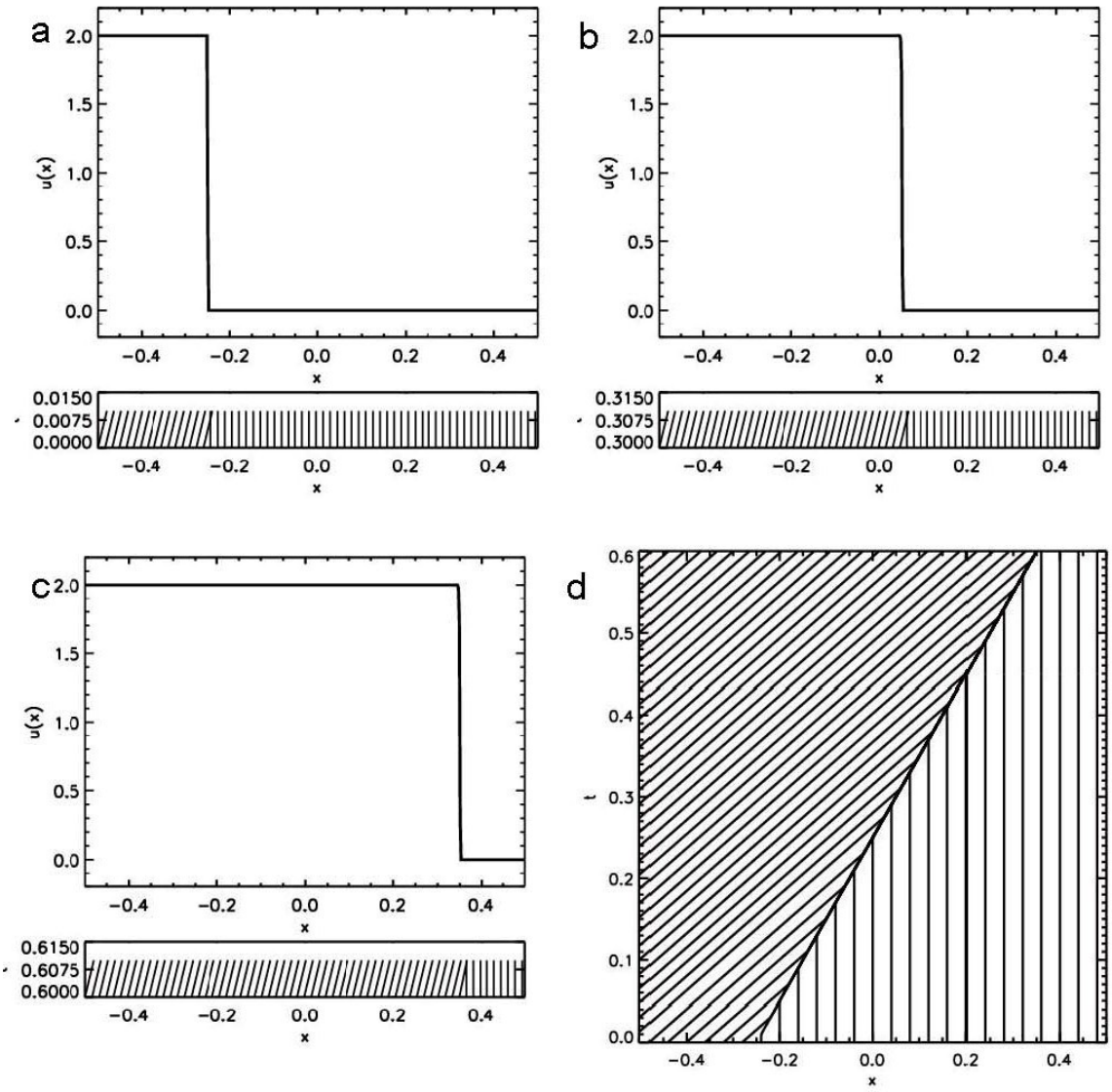

Figs. 4.5a to 4.5c show the propagation of a shock using Burgers equation at times of 0, 0.3 and 0.6 respectively. The panel below each plot shows the time evolution of the characteristics for a short time interval, i.e. 0.01, after the times shown. Notice that the characteristics always intersect showing that the shock is propagating. Fig. 4.5d shows the characteristics in space-time. The line where the characteristics from the left and right intersect defines the location of the shock.

The previous paragraph showed that shocks can form for certain initially discontinuous solutions. But do they form for all possible initially discontinuous solutions? In this paragraph we study the evolution of discontinuous initial conditions given by $u_0(x) = 0$ for $x < -0.25$ and $u_0(x) = 0.5$ for $x \geq -0.25$. Notice that the initial

conditions are constant on either side of the initial discontinuity. Fig. 4.6 shows the solution in the interval $[-0.5, 0.5]$. Observe too that the characteristic speeds to the left and right of the initial discontinuity are given by $f'(0) = 0$ and $f'(0.5) = 0.5$, i.e. the initial characteristics are flowing away from the discontinuity. The evolution of this profile at times $t = 0,\ 0.5$ and 1.0 is shown in Figs. 4.6a through 4.6c . The panel at the bottom of each of those figures displays a small space-time plot showing the evolution of the characteristics in space-time for 0.1 units of time after the time at which the solution is shown in each of those figures. The panel at the bottom of Fig. 4.6a should be compared to the analogous panel at the bottom of Fig. 4.5a. The important difference is that in Fig. 4.5a the characteristics converge into each other at $x = -0.25$ and $t = 0$ whereas the characteristics in Fig. 4.6a diverge at the same space-time point. As a result, we expect the evolution of the discontinuous initial conditions to be different. Figs. 4.6b and 4.6c show that the evolution is indeed different. Unlike the shock solution the profile of the rarefaction wave evolves as a continuous solution for $t > 0$. The rarefaction wave is also a differentiable solution except at its end points where it connects with the left and right constant states. Fig. 4.6d shows the evolution of the characteristics in space-time. We see from Fig. 4.6d that the leftmost characteristic that emanates from $x = -0.25$ at $t = 0$ propagates along the line $x = -0.25$ because the wave speed in the left state is zero. The rightmost characteristic that emanates from the point $x = -0.25$ at $t = 0$ propagates along the line $x = -0.25 + 0.5\,t$ because the wave speed in the right state is 0.5. The remaining characteristics emerging from $x = -0.25$ at $t = 0$ form a fan-like structure, giving the name *rarefaction fan* to the resulting structure.

The effect of the rarefaction fan shown in Fig. 4.6d is reflected in Figs. 4.6b and 4.6c which show the ends of the rarefaction fan propagating away from each other at a uniform speed. The solution between the ends of the rarefaction fan in Figs. 4.6b and 4.6c can indeed be seen to evolve in a self-similar fashion. In other words, the solution in Fig. 4.6b stretches out in time to become the solution displayed in Fig. 4.6c. This self-similar evolution is made possible by the diverging characteristics seen in Fig. 4.6d . By starting from the characteristic line $x = -0.25$ and sequentially progressing to the characteristic

line $x = -0.25 + 0.5\,t$ in Fig. 4.6d, we see that the slopes of the diverging characteristics increase. For Burgers equation Fig. 4.3 shows us that the slope of the characteristic is exactly equal to the value of the solution carried by that particular characteristic. As a result, Fig. 4.6d shows us that the family of diverging characteristics that start at $x = -0.25$ and incrementally progress to $x = -0.25 + 0.5\,t$ indeed carry increasing values of the solution; and this is reflected in the solutions shown in Figs. 4.6b and 4.6c.

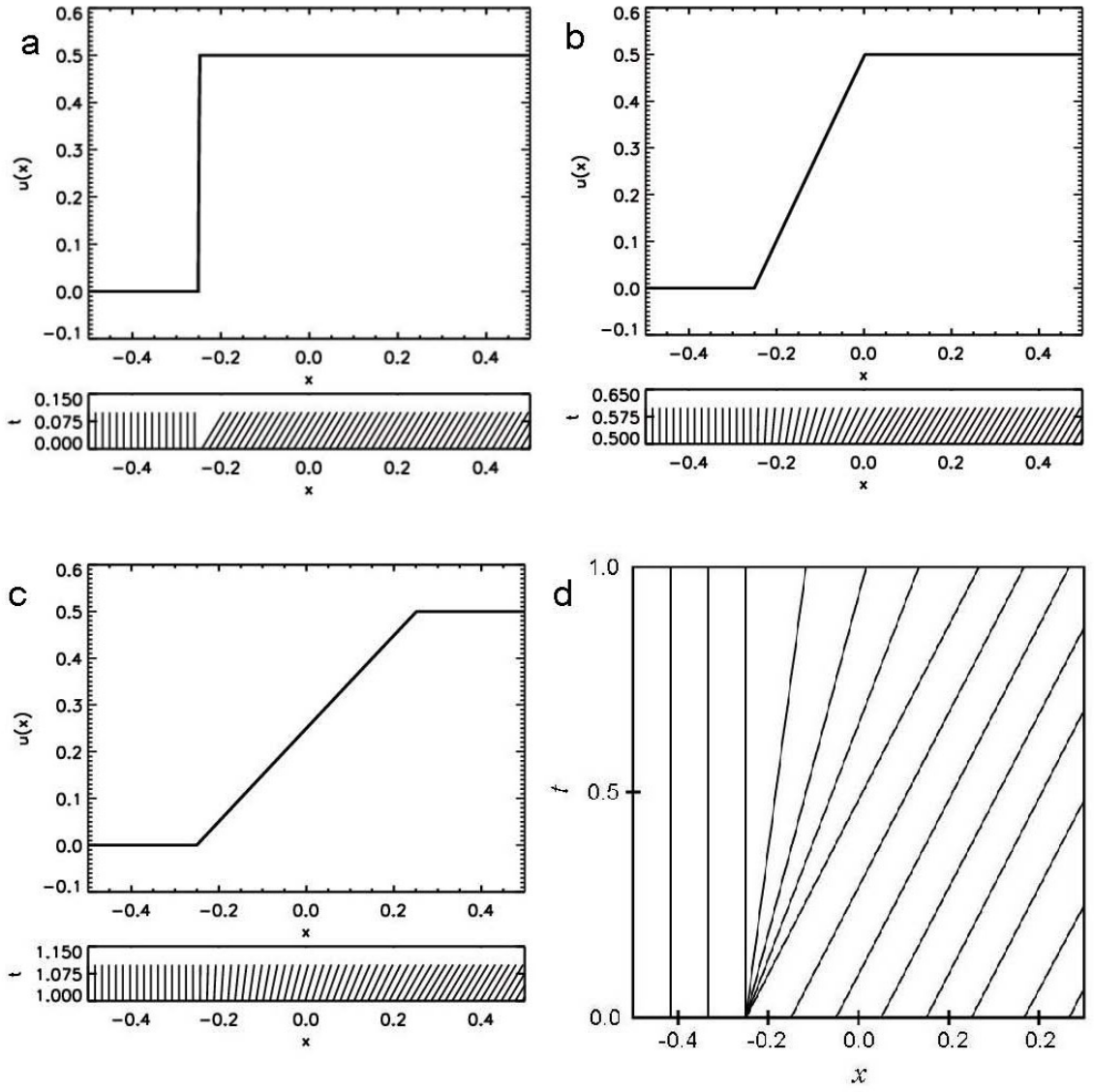

Figs. 4.6a to 4.6c show the propagation of a rarefaction fan using Burgers equation at times of 0, 0.5 and 1.0 respectively. The panel below each plot shows the time evolution of the characteristics for a short time interval, i.e. 0.1, after the times shown. Notice that the characteristics always diverge showing that a rarefaction wave is propagating. Fig. 4.6d shows the characteristics in space-time. The characteristics that form the rarefaction fan emanate from the initial discontinuity.

To summarize this sub-section, we see that piecewise constant initial conditions with a single discontinuity in them can give rise to isolated shocks or rarefaction fans depending on whether the characteristics converge into the discontinuity or diverge away

from it. Both isolated shock waves and isolated rarefaction fans are *self-similar* solutions of a hyperbolic conservation law. They are analogous to the simple waves that we studied in Sub-Section 3.4.2. In fact, we say that isolated shocks and rarefactions are indeed the *simple wave solutions* of our non-linear scalar conservation law. We will see later on that self-similarity is a very useful concept that enables us to derive the detailed structure of shocks and rarefaction fans. The speed with which an isolated shock propagates depends on the flux function. Similarly, the flux function also determines the structure of a rarefaction fan. In the next chapter we will see that systems of non-linear hyperbolic conservation laws also support simple wave solutions that are self-similar. Even for systems of hyperbolic conservation laws, we will find that these simple waves can be initialized with carefully chosen piecewise constant initial conditions with a single discontinuity. Whether we get simple wave solutions that are shocks or rarefactions will again depend on whether the characteristics initially flow into each other or whether they flow away from each other. In the next two sections we study the mathematical structure of isolated shocks and rarefaction fans.

Example of a Non-Convex Flux

This section has mainly focused on hyperbolic equations with convex flux functions. Hyperbolic systems with non-convex fluxes can also arise in science and engineering. A good example of a scalar hyperbolic system with a non-convex flux would be the Buckley-Leverett equation which arises in the modeling of a multi-phase mixture of water and oil. The flux in eqn. (4.1) is then given by

$$f(u) = \frac{4u^2}{4u^2 + (1-u)^2}$$

The wave propagation speed is then given by

$$f'(u) = \frac{8\,u\,(1-u)}{\left[4\,u^2 + (1-u)^2\right]^2}$$

We see that $f'(0) = f'(1) = 0$ and $f'(u) > 0$ for 0<u<1 so that the flux is non-convex when "u" lies in the interval $[0,1]$. At $u \sim 0.287$, $f'(u)$ has a maximum. We similarly see that $\lim_{u\to\infty} f'(u) = 0$ so that the flux is also non-convex for "u" lying in the interval $[1,\infty]$.

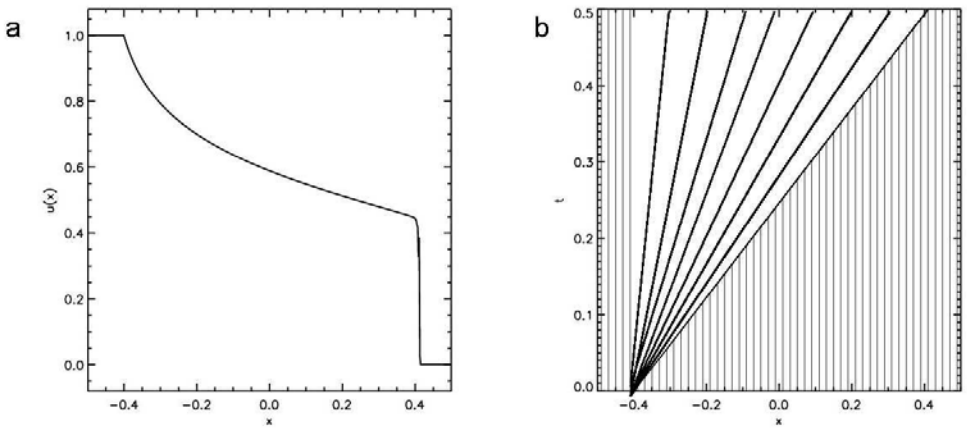

The figure on the left shows the solution at t=0.5 for the Buckley-Leverett problem with the initial conditions catalogued in the text. We see the formation of a compound wave with a right-going shock and a rarefaction fan attached behind it. The figure on the right shows the characteristics in space-time.

We initialize this problem with the discontinuous solution $u_0(x) = 1$ for $x < -0.4$ and $u_0(x) = 0$ for $x \geq -0.4$ on the unit interval $[-0.5, 0.5]$. The figure on the top shows the solution at $t = 0.5$. The evolution of the characteristics in space-time is also shown. We see that the solution consists of a right-propagating shock with a rarefaction attached to it. Such a solution is a direct result of the non-convex flux and is known as a *compound wave*. The compound wave in this case consists of a right-going shock with a rarefaction fan of the same family attached to it.

The emergence of a compound wave is fundamentally a consequence of the non-convexity of the flux function $f(u)$. Notice that when the flux is convex the propagation speed $f'(u)$ varies monotonically with increasing/decreasing values of "u". This guarantees that all shocks are compressive shocks, i.e. all the waves of a given family from both sides of a shock go into the shock, as was the case in Figs. 4.4e and 4.5d. Briefly consider Fig. 4.5d for the Burgers equation. Increasing the value of the solution in the post-shock region can only result in a stronger shock because it only increases the speed with which the characteristics in the post-shock region flow into the shock. As a result, when starting from an initial discontinuity between two constant states, the Burgers equation will never produce a self-similar solution where a rarefaction fan remains affixed to a shock. When the hyperbolic system is non-convex we cannot guarantee such a monotone variation of the characteristic speed with the value of the solution. As a result, we could form compound wave solutions for the Buckley-Leverett equation.

The right panel of the above figure displays the characteristics around a compound shock. We see that the shock solution continuously goes over to a rarefaction fan, i.e. the characteristics from both sides of the shock do not go into the shock. If the physical problem is prone to developing compound shocks then it behooves the alert computationalist to be aware of their existence. Their presence will have to be accounted for in the numerical technique that one designs for solving hyperbolic problems with a non-convex flux function. The compound shocks that are analogous to the ones displayed here are also known to arise in non-relativistic as well as relativistic MHD flow and we will discuss compound shocks that arise for the MHD system in Chapters 6 and 8.

4.3) Isolated Shock Waves

In this section, we study shock waves from two equivalent viewpoints. Sub-section 4.3.1 shows us shock waves as the inviscid limit of a solution of a viscous

equation. Sub-section 4.3.2 presents shock waves as weak solutions of a hyperbolic equation.

4.3.1) Shocks as Solutions of Viscous Equations that are Taken to the Inviscid Limit

In the previous section we showed that discontinuous solutions can arise from smooth initial conditions when the hyperbolic equation is non-linear. We also claimed that the discontinuous solution is indeed a physical solution. The existence of discontinuous solutions always seems a little strange when it is first introduced. Let us, therefore, justify it by appealing to the physics of an example problem. Consider a shock that forms in a gas. In reality, the atoms or molecules that make up any gas have to undergo collisions. In Chapter 1 we have seen that it is impossible to justify a fluid dynamical approximation without drawing on the fact that collisions occur on length scales and time scales that are much smaller than the physical scales of the problem. These collisions ensure that the velocities of the atoms follow a Boltzmann distribution when viewed in the fluid's own rest frame. Our derivation of the fluid dynamic equations is predicated on the existence of such a locally Boltzmannian distribution. The existence of atomic or molecular collisions also ensures that non-ideal effects always occur on some small scale in the problem. On those scales non-ideal effects such as viscosity, thermal conduction do indeed become important. These effects contribute parabolic terms to our PDE. Thus the actual PDE that we are studying is not hyperbolic but rather parabolic. The hyperbolic structure of the Euler equations is only realized when we ignore the smaller scales on which the parabolic terms dominate the problem. However, if the solution of a non-linear problem self-steepens to form a shock, then we cannot ignore the small scales on which non-ideal, i.e. viscous, terms operate in the vicinity of the shock. The viscous terms model atomic collisions and such collisions are needed in order to raise the entropy of a parcel of fluid that passes through a shock, see eqn. (1.38). Since it is the nature of parabolic equations to smooth out discontinuities, the shock's profile will, therefore, always be smoothed out on the viscous scales. On those very small viscous scales, the shock profile indeed has a finite thickness that is proportional to the distances over which atomic or molecular collisions operate. A shock only needs to be

treated as a discontinuity if we choose to simultaneously ignore the viscous terms in our governing equations as well as the viscous length scales in the physical problem. This is done by making the problem hyperbolic.

Let us, therefore, study the viscous form of the Burgers equation. It is given by

$$\mathrm{u}_t + \left(\frac{\mathrm{u}^2}{2} \right)_x = \eta \, \mathrm{u}_{xx} \tag{4.7}$$

where the viscosity η has units of a length times a velocity. If the above equation is derived from the Navier-Stokes equations then, like all transport coefficients, η should be proportional to the product of the thermal velocity of the atoms that make up the fluid and the mean free path of the atoms. As a result, in regions of smooth flow, the left hand side of eqn. (4.7), i.e. the hyperbolic part, dominates. However, when discontinuities form on length scales that are comparable to the mean free path, the right hand side of eqn. (4.7), i.e. the parabolic part, dominates. Overall, eqn. (4.7) has a parabolic character and should always yield smooth solutions. We wish to study solutions of eqn. (4.7) that tend to a constant value u_L for $x \ll 0$ and another constant value u_R for $x \gg 0$. For $\mathrm{u}_L > \mathrm{u}_R$ it can be shown via substitution that one possible solution of eqn. (4.7) is given by

$$\mathrm{u}(x,t) = \mathrm{u}_R + \frac{1}{2}(\mathrm{u}_L - \mathrm{u}_R)\left\{ 1 - \tanh\left[\frac{(\mathrm{u}_L - \mathrm{u}_R)}{4\eta} \left(x - \frac{1}{2}(\mathrm{u}_L + \mathrm{u}_R)t \right) \right] \right\} \tag{4.8}$$

Fig. 4.7 shows this profile at a time $t = 1$ with different values of η and with $\mathrm{u}_L = 2$ and $\mathrm{u}_R = 0$. We display plots for $\eta = 0.5,\ 0.2,\ 0.05$ as well as the inviscid solution $\eta = 0$. We see that as $\eta \to 0$ the solution tends towards a shock profile with initial conditions specified at $t = 0$ by a constant left state given by $\mathrm{u}_0(x) = \mathrm{u}_L = 2$ for $x < 0$ and a

constant right state given by $u_0(x) = u_R = 0$ for $x \geq 0$. We therefore refer to the solution in eqn. (4.8) as a *viscous shock*.

The Navier-Stokes equations also support viscous shock solutions which display compelling parallels with the viscous shock solution in eqn. (4.8). We list them here. First, the structure of the viscous shock represents a competition between the non-linear terms on the left hand side of eqn. (4.7), which try to self-steepen the profile, and the viscous terms on the right hand side of eqn. (4.7) which try to smooth it out. Similar competing effects act on viscous hydrodynamical shocks where the non-linear terms in the velocity equation try to steepen a shock profile and the viscous terms try to smooth it out. As the viscosity is reduced for the same initial conditions, the shock profile steepens as is seen from Fig. 4.7. Recall that Fig. 4.5 has already shown us the time evolution of the inviscid solution with these left and right states. Second, we see that all the viscous shocks in Fig. 4.7 as well as their inviscid counterpart travel with the same speed $(u_L + u_R)/2$. Viscous shocks arising from the Navier-Stokes equations also propagate at the same speed as the inviscid shocks arising from the Euler equations. Third, an examination of eqn. (4.8) further shows that as the shock jump $(u_L - u_R)$ increases for the same viscosity η the width of the viscous shock, which is given by $4\eta/(u_L - u_R)$, becomes narrower. This trend is also seen in the viscous shocks arising from the Navier-Stokes equations. Viscous shock profiles for the Navier-Stokes equations are derived in Landau & Lifshitz (1987) .

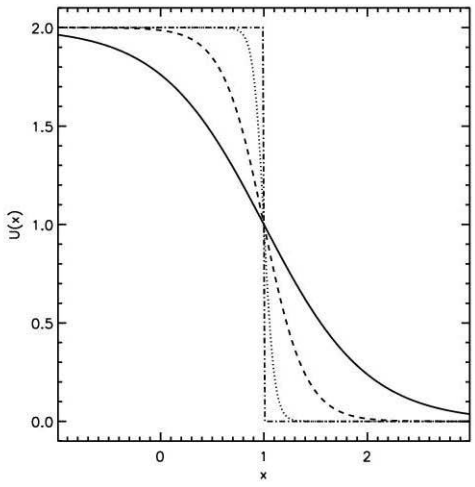

Fig. 4.7 shows the viscous shock profiles arising from the viscous Burgers equation at a time t=1 with different values of η *and with* u_L *= 2.0 and* u_R *= 0.0 . We display plots for* η*=0.5, 0.2 and 0.05 as the solid, dashed and dotted curves respectively. We also show the inviscid solution with* η *= 0 as a dot-dashed curve .*

Having seen that there is a physically meaningful resolution for the discontinuities associated with shock waves, it is also worth pointing out that the viscous scales on which shock profiles are smooth are indeed many orders of magnitude smaller than the scales that are simulated. It is usually not practical to simulate the small viscous scales in most science and engineering problems. For example, strong hydrodynamical shocks can assume a width that is comparable to the mean free path of the molecules in a gas. For air at normal temperature and pressure, the mean free path can be as small as 10^{-4} cm, a scale which cannot be retained in practical engineering simulations. Consequently, we are willing to accept shocks as discontinuous solutions of our hyperbolic conservation laws.

4.3.2) Shocks as Weak Solutions of a Hyperbolic Equation

In light of the previous paragraph, we wish to find weak solutions for shock discontinuities by using an integral formulation that is similar to the one in Fig. 3.9 and eqns. (3.32) to (3.35) of Chapter 3. As in Chapter 3, we realize that eqn. (4.1) cannot by itself represent a discontinuous solution because the derivatives are ill-defined. Thus imagine a situation where we have $u_0(x) = u_L$ for $x < 0$ and $u_0(x) = u_R$ for $x \geq 0$. Let that discontinuity propagate from the origin in the *x*-direction so that at a time "T" it has propagated a distance "X" as shown in Fig. 4.8. Our prior experience tells us that the propagation is self-similar, so the discontinuity traces out a straight line in space-time.

We can now integrate $u_t + f(u)_x = 0$ over the rectangle $[0, X] \times [0, T]$ in space and time, see Fig. 4.8. Using integration by parts we get

$$\begin{aligned} & u_L\ X\ -\ u_R\ X + f(u_R)\ T\ -\ f(u_L)\ T = 0 \ \Leftrightarrow \\ & f(u_R)\ -\ f(u_L) = \frac{X}{T}\ (u_R - u_L) \end{aligned} \tag{4.9}$$

Owing to the self-similarity of the problem we can identify the shock speed "s" with "X/T" in eqn. (4.9) above. When we replace "X/T" by the shock speed "s" in eqn. (4.9) we obtain is the *Rankine-Hugoniot jump condition* for scalar conservation laws. Recall, therefore, that we obtained a similar jump condition from the integral form of the conservation law when we studied simple waves in Sub-section 3.4.2. In the next chapter we will see that the concept extends to systems of hyperbolic conservation laws. We now use eqn. (4.9) to obtain an expression for the shock speed as

$$s = \frac{f(u_R) - f(u_L)}{u_R - u_L} = \frac{[f(u)]}{[u]} \tag{4.10}$$

where we define the jumps $[f(u)] \equiv f(u_R) - f(u_L)$ and $[u] \equiv u_R - u_L$. The form of the flux function determines the shock speed. For the Burgers equation, it is easy to show that the shock speed is $(u_L + u_R)/2$ and is concordant with the viscous shock speed from eqn. (4.8). For weak shocks, i.e. when $u_R \to u_L$, it is possible to show quite generally that $s \to f'((u_L + u_R)/2)$ and the result is independent of the form of the flux function. Thus as a shock discontinuity weakens, the shock speed smoothly tends to the characteristic speeds on either side of it. This is as one would physically expect. Eqn. (4.10) is also valid for non-convex flux functions. Recall from our example of the non-convex Buckley-Leverett equation that shocks can have adjoining rarefaction fans. Consequently, in such situations we have to pick u_L to be the value that is immediately

to the left of the discontinuity and u_R to be the value that is immediately to the right of the discontinuity.

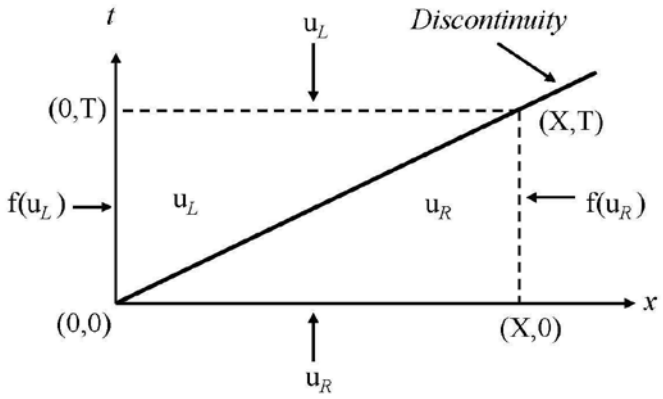

Fig. 4.8 shows a propagating shock wave in space-time. It propagates a distance X *along the x-axis in a time* T. *The non-linear hyperbolic equation is integrated over the rectangle shown by the dashed line. The values of the solution at the upper and lower boundaries of the rectangle are shown in the figure, as are the fluxes at the rectangle's left and right boundaries.*

Owing to the use of the fluxes in eqn. (4.10) we see that the conservation form of the hyperbolic system is indeed the most fundamental form of the hyperbolic system. The conservation form is the only form of the hyperbolic equation that admits discontinuous, weak solutions. As with the Burgers equation, we have seen that hyperbolic equations can be written in alternative forms. However, since our goal is to develop methods for hyperbolic systems in conservative form that can capture discontinuous shock solutions, we will always use the conservation form of the PDE for the numerical update of these equations on a computational domain. Chapter 1 has shown that fluids satisfy conservation of mass, momentum and energy and our use of a conservation form in numerical codes ensures that those same continuous symmetries are respected at the discrete level by the numerical method. The methods we will develop are said to be in *flux conservative form* and such methods are also *locally conservative*, i.e. they ensure that if some amount of mass, momentum or energy is transported from one zone to its neighbor then there is a *detailed balance* in the amount of that variable lost by the first zone and gained by its neighbor.

The Connection Between Hyperbolic and Parabolic Equations

There is a very interesting connection between dissipation in numerical methods for hyperbolic equations and parabolic systems. Consider the scalar hyperbolic equation $u_t + f(u)_x = 0$. Oleinik (1957) was able to show that provided the flux f(u) is convex, the physically consistent discontinuous solutions for this equation are those obtained from the corresponding parabolic equation $u_t + f(u)_x = \eta\, u_{xx}$ in the limit where the diffusion coefficient $\eta \to 0$. In practice, this means that the parabolic equation, by virtue of its dissipation term, produces non-oscillatory solutions even when the initial conditions have a discontinuity, see Fig. 2.9 for example. Consequently, Oleinik's theorem tells us that the resolution of a discontinuity for a hyperbolic system should also produce a solution that is free of new wiggles. Oleinik's work provides a very sound physical basis for the TVD property which is incorporated into schemes for solving hyperbolic equations.

Ironically, Oleinik's theorem also provides a justification for the older *parabolized schemes* for treating hyperbolic flows. Such parabolized schemes introduce an extra dissipation term in strongly shocked regions using an *artificial viscosity*. The artificial viscosity is patterned after the physical viscosity but the viscosity coefficient only assumes large values in the vicinity of shocks. Such an artificial viscosity is often referred to as the *vonNeumann-Richtmeyer viscosity*. This makes the scheme parabolic in regions where the artificial viscosity is invoked. The parabolized schemes, therefore, parallel Oleinik's introduction of a viscosity in her theorem in order to stabilize the shock waves that might form.

To work well, the parabolized schemes have to look at solution-dependent structures, such as the divergence of the velocity in a fluids code, to detect the location of discontinuities and artificially raise the numerical viscosity in that location. Parabolized schemes do, however, face the difficulty that their artificial viscosity formulations may not pick out every physical discontinuity that forms in the flow. For example, finite amplitude torsional Alfven waves that form in the MHD system do not produce an associated change in the velocity of the flow. As a result, torsional Alfven waves slip through the net cast by the discontinuity detector in artificial viscosity based schemes.

Consequently, parabolized schemes for MHD have to resort to unconventional strategies for dealing with such flow structures.

4.4) Isolated Rarefaction Fans

The previous section presented a shock wave as a self-similar solution that arises from a single, isolated discontinuity in the initial conditions. However, Fig. 4.6 has shown that not all discontinuities result in shock waves. Certain types of discontinuous initial conditions can even yield self-similar rarefaction fans. This happens when the characteristics propagate away from the initial discontinuity. We, therefore, study rarefaction fans in this section. Sub-section 4.4.1 introduces the structure of an isolated rarefaction fan. Sub-section 4.4.2 explores the role of entropy in determining the evolution of discontinuous initial conditions.

4.4.1) The Structure of an Isolated Rarefaction Fan

In order to understand rarefaction fans, let us consider an initial discontinuity specified at the origin at $t = 0$ by a constant left state given by $\mathrm{u}_0(x) = \mathrm{u}_L$ for $x < 0$ and a constant right state given by $\mathrm{u}_0(x) = \mathrm{u}_R$ for $x \geq 0$. Let us restrict attention to a convex flux function and let us also require $\mathrm{f}'(\mathrm{u}_L) < \mathrm{f}'(\mathrm{u}_R)$ so that the initial discontinuity opens up as a rarefaction fan. Fig. 4.6 has shown us that the solution is self-similar. We therefore explore self-similar solutions that emanate from the origin; i.e. we want solutions that depend on only one self-similarity variable $\xi \equiv x/t$ instead of the two variables "*x*" and "*t*". We can then write the solution as

$$\mathrm{u}(x,t) = \tilde{\mathrm{u}}(\xi) = \tilde{\mathrm{u}}(x/t) \quad \text{where} \quad \xi \equiv x/t \tag{4.11}$$

Fig. 4.6 has shown us that for $t > 0$ the structure of the rarefaction fan is such that we can obtain well-formed spatial and temporal derivatives inside the rarefaction fan. Note though that this is not true at either extremity of the rarefaction fan where the spatial

derivatives become ill-defined. Denoting $\tilde{u}'(\xi) \equiv d\,\tilde{u}(\xi)/d\xi$ we can now write the temporal and spatial derivatives of $u(x,t)$ and $f(x,t)$ inside the rarefaction fan as

$$u_t(x,t) = -\frac{x}{t^2}\tilde{u}'(\xi) \quad \text{and} \quad f_x(x,t) = \frac{1}{t} f'(\tilde{u}(\xi))\,\tilde{u}'(\xi) \tag{4.12}$$

Inside the rarefaction fan, the solution is differentiable for $t > 0$ so that the non-conservative form of eqn. (4.1), which is given by $u_t + f'(u)\,u_x = 0$, still holds. Substituting the derivatives from eqn. (4.12) in the non-conservative form of eqn. (4.1) yields

$$f'(\tilde{u}(\xi)) = \xi \tag{4.13}$$

Eqn. (4.13) gives us the solution of a rarefaction fan and is only valid in the interior of the fan, i.e. for $f'(u_L) < \xi < f'(u_R)$. Physically, eqn. (4.13) means that the characteristics are straight lines in space-time; see Fig. 4.6d. The solution assumes a constant value along each of those characteristics though different characteristics could carry solutions with different values. At the end points of the rarefaction fan, given by the characteristic lines $x = f'(u_L)\,t$ and $x = f'(u_R)\,t$, the rarefaction wave has to join continuously to the constant left and right states respectively.

To take the Burgers equation as an example, eqn. (4.13) gives us $f'(u) = u$ so that our solution for the rarefaction fan is simply $u(x,t) = x/t$. At $x = u_L\,t$ and $x = u_R\,t$ this rarefaction fan for the Burgers equation joins with the states u_L and u_R respectively.

4.4.2) The Role of Entropy in Arbitrating the Evolution of Discontinuities

Our study of solutions of hyperbolic equations with discontinuous initial conditions immediately brings up a question: Is there any way of deciding which of the

possible discontinuous initial conditions form rarefactions and which ones form shocks? Notice that we could, for the sake of argument, make the claim that all discontinuous initial conditions should form a shock that propagates with a speed given by eqn. (4.10). The resulting solution would indeed satisfy the hyperbolic equation, i.e. eqn. (4.1), in a weak sense. But we know that certain discontinuous initial conditions give rise to rarefaction waves. Clearly, there has to be some extra bit of physics that decides which discontinuous initial conditions yield rarefaction fans and which ones form shocks. That extra bit of physics is provided to us by considering the principle of entropy generation. Thus consider the evolution of Burgers equation with the same initial conditions ($\mathrm{u}_0(x) = 0$ for $x < -0.25$ and $\mathrm{u}_0(x) = 0.5$ for $x \geq -0.25$) that were used in Fig. 4.6. Say, for the sake of argument, that we now demand that a shock solution be fitted to this discontinuous initial data. Eqn. (4.10) would then tell us that a shock wave propagates to the right with a shock speed of $1/4$. The characteristics emanating from such a shock are shown in Fig. 4.9. We see that new characteristics emerge from the shock as it propagates. Since we have interpreted characteristics as rays in space-time that carry information, we see from Fig. 4.9 that new information is being generated at the shock. This is unphysical, and such shocks do not occur in nature. While such a shock is fictitious, we call it a *rarefaction shock* because we will see that numerical algorithms that do not take steps to prohibit the emergence of such rarefaction shocks can indeed produce such unphysical shocks in certain circumstances.

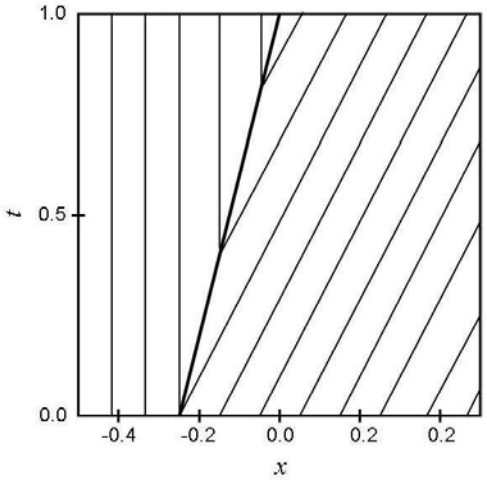

Fig. 4.9 shows the characteristics that result from a rarefaction shock. The rarefaction shock is shown with a thick line. It is obtained by asserting a shock solution for the same initial conditions that were shown in Fig. 4.6. Notice that the characteristics emanate from the rarefaction shock. This is an unphysical, entropy-violating solution that never occurs in nature.

The Euler equations indeed have an explicit form for the thermodynamic entropy. Thus if we impose a condition that any physical solution of the Euler equations should satisfy the second law of thermodynamics, we should be able to rule out rarefaction shocks. We will see this via a problem at the end of the next chapter. In fact, Harten (1983b) was able to draw on a numerical form of the entropy that is quite like the physical entropy to prove that certain types of schemes for the numerical solution of the Euler equations do indeed converge to the entropy-satisfying physical solution. We even realize that the existence of a physical viscosity on small scales will always smooth out an initial discontinuity and thus make it possible for the discontinuity to evolve as a rarefaction fan in an entropy-satisfying fashion.

While nature provides us with a physical entropy for the Euler system, there are many hyperbolic systems, such as the Burgers equation or the Buckley-Leverett equation, that do not have a physically motivated entropy. Mathematicians have, therefore, been able to formulate entropy functions and they have been able to define *entropy conditions* which allow them to identify physically admissible solutions. Such entropy conditions are, therefore, also called *admissibility conditions*. However, it is not possible to define such entropy conditions for all different types of hyperbolic conservation laws. For convex, scalar, conservation laws, Lax (1972) was able to formulate an entropy condition. Lax's condition says that a physically admissible discontinuity propagating with a speed "*s*" in accordance with eqn. (4.10) must satisfy the further condition $f'(u_L) > s > f'(u_R)$ where u_L and u_R are the values of the solution to the left and right of the discontinuity. *Lax's entropy condition* closely parodies the flow of characteristics into a hydrodynamical shock, as we will see in the next chapter. Notice that for Burgers equation, which is a convex, scalar, conservation law, we have $s = (u_L + u_R)/2$. Consequently, Lax's theorem excludes entropy violating shocks, i.e. shocks with $u_L < u_R$, from being physically realizable solutions of Burgers equation. For example, the discontinuity in Fig. 4.9 has $f'(u_L = 0) = 0$, $s = 0.25$ and $f'(u_R = 0.5) = 0.5$; thus it does not satisfy Lax's entropy condition. Oleinik (1957, 1964) was able to formulate a

generalized entropy condition for all scalar conservation laws. Her entropy condition is applicable to convex and non-convex flux functions.

Harten (1983b) showed that all symmetrizable hyperbolic systems admit a numerically-motivated entropy condition. We will not explore the details of symmetrizable hyperbolic systems here. The reader might find it useful to know that the Euler equations can be written in such a symmetrizable form, the MHD equations cannot. (However, a modified version of the MHD equations can indeed be written in symmetrizable form, as was first shown by Godunov.) We see, therefore, that the support provided to us by firmly grounded mathematical theories is indeed incomplete. However, the insights we have gained from such mathematical studies are useful and often generally applicable. Since the different entropy conditions alluded to out here can only be explicitly demonstrated by proving detailed theorems, we do not discuss the details further in this text. Readers who want more mathematical details on entropy conditions can go through the references cited in this section.

Example of Shock-Rarefaction Interaction

In order to develop a better understanding of shocks and rarefactions we consider a simple problem that demonstrates their interaction. Thus consider the solution of the Burgers problem with initial conditions given by $\mathrm{u}_0(x) = 1$ for $0 < x < 1$ and $\mathrm{u}_0(x) = 0$ for all other points on the x-axis. The space-time diagram for the characteristics is given below. It shows that a shock emerges from the point $x = 1$ at time $t = 0$ and propagates for at least a finite duration of time with a speed of 0.5. The space-time location of the shock for at least some time after $t = 0$ is given by $x = 0.5\,t + 1$. At the point $x = 0$ at time $t = 0$ we also see the emergence of a rarefaction fan with a solution $\mathrm{u}(x,t) = x/t$. For at least a short time after its emergence, the rarefaction fan is bounded by the characteristic lines $x = 0$ and $x = t$ in space-time. The shock and rarefaction fan propagate without interacting for some time. However, eventually the rightmost characteristic of the rarefaction fan, which is given by $x = t$, intersects with the locus of

the shock, which is given by $x = 0.5\,t + 1$. This happens at $(x,t) = (2,2)$. For times $t > 2$ the shock and rarefaction fan interact with each other. We wish to find the locus of the shock , $x_s(t)$, for $t > 2$. Notice that we also require $x_s(2) = 2$ so that the locus of the shock matches with the point where the rarefaction fan and shock had their first interaction.

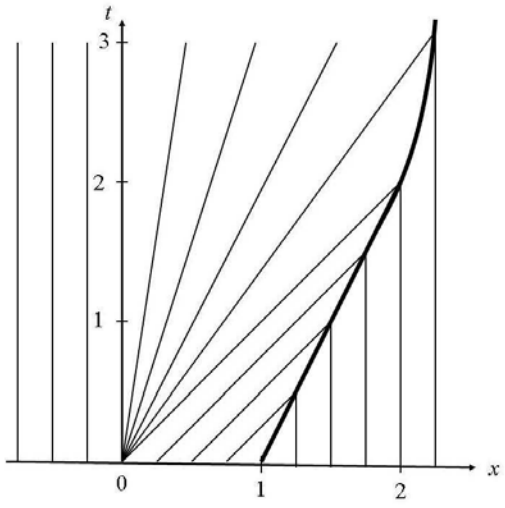

The figure shows the space-time diagram for the evolution of the characteristics in the shock-rarefaction intersection problem. The shock is shown by the thick curve. The initial conditions at time t=0 are $u_0(x)=1$ for $0<x<1$ and $u_0(x) = 0$ otherwise. The shock and rarefaction fan begin to interact at (x,t) = (2,2). For t>2 the locus of the shock is no longer a straight line. This is because the instantaneous left state of the shock keeps changing as different parts of the rarefaction fan come into interaction with the shock.

The space-time diagram for the evolution of the characteristics shows us that for $t > 2$ the left state of the shock is always set by the rarefaction fan while the right state continues to be $u_R = 0$. The shock slows down because its left state has a decreasing value as time progresses, as can be seen from the figure. Since the left state of the shock is some interior location in the rarefaction fan, we can write the left state as $u_L = x_s(t)/t$. The shock locus then satisfies the instantaneous shock jump conditions so that eqn. (4.10) gives us

$$\frac{d\,x_s(t)}{d\,t} = \frac{\frac{1}{2}\left(\frac{x_s}{t}\right)^2 - \frac{0^2}{2}}{\left(\frac{x_s}{t}\right) - 0} = \frac{1}{2}\left(\frac{x_s}{t}\right)$$

The solution of the above ordinary differential equation that is consistent with the initial conditions is then given by $x_s(t) = 2(t/2)^{1/2}$.

4.5) The Entropy Fix and Approximate Riemann Solvers

In the previous two sections we undertook a systematic study of shocks and rarefaction problems because they are useful in the design of Riemann solvers. Sub-Section 3.4.3 has already shown us the utility of Riemann solvers for linear hyperbolic systems. This section shows us the utility of Riemann solvers in the numerical solution of scalar conservation laws with non-linear fluxes. Sub-Section 4.5.1 demonstrates the importance of the entropy conditions for obtaining a physically consistent numerical flux. Sub-Section 4.5.2 gives us our first introduction to approximate Riemann solvers for scalar conservation laws.

4.5.1) The Entropy Fix

In Section 3.4.3 we saw that a numerical implementation of linear hyperbolic systems has the same characteristic structure at all the zone boundaries. The presence of non-linearities changes the structure of the Riemann problem at the zone boundaries. For non-linear, scalar, conservation laws, the characteristics that emanate from discontinuous initial conditions depend on the values of the solution at the left and right sides of the discontinuity. I.e., the Riemann problem becomes solution-dependent. Fig. 4.10, which should be contrasted with the lower panel in Fig. 3.11, schematically shows Godunov's method on a one-dimensional mesh. The figure shows the evolution in space and time of the Riemann problems at each zone boundary. The thick solid lines show shocks while the dashed lines display rarefaction fans. To find the *numerical flux* at those zone boundaries, we first need to obtain the *resolved state* that overlies the zone boundary. The resolved state is given by the value of the solution at the zone boundary. The *resolved flux* can be computed by evaluating the flux function for the value of the resolved state. We see that zone boundaries $i-3/2$ and $i-1/2$ have a left-going shock and a left-going

rarefaction fan respectively. Thus the resolved state at those boundaries is just the value of the solution immediately to the right of the respective boundary. Similarly, the zone boundaries $i+3/2$ and $i+5/2$ have a right-going rarefaction fan and a right-going shock respectively. The resolved state at those boundaries is just the value of the solution immediately to the left of the respective boundary. The zone boundary $i+1/2$ is interesting because the rarefaction fan straddles it. Thus we have to evaluate the inner structure of the rarefaction fan using the results from Section 4.4 in order to get the correct resolved state. Once the resolved state that overlies a zone boundary is obtained, we can evaluate the resolved, numerical flux for that zone boundary.

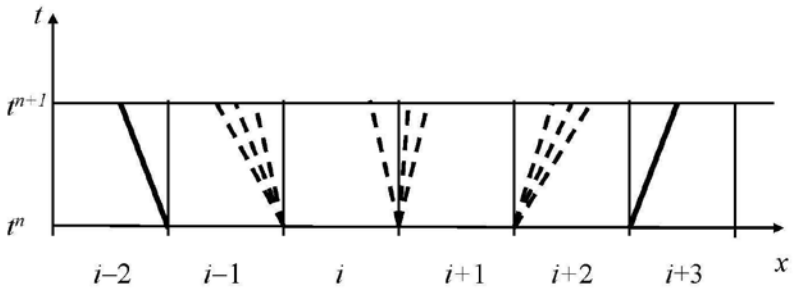

Fig. 4.10 schematically shows Godunov's method on a one-dimensional mesh where each zone is represented as a slab of fluid. The figure shows the evolution in space and time of the Riemann problems at zone boundaries. The thick solid lines show shocks while the dashed lines show rarefaction fans. Because the problem is non-linear, the Riemann problems can have different configurations with respect to the zone boundary. The resolved state is given by the value of the solution at the zone boundary. The resolved flux can be computed from the resolved state.

We see from Fig. 4.10 that evaluating the resolved state at all zone boundaries that are not straddled by a rarefaction fan is indeed easy. I.e. we either pick the value on the immediate right of the zone boundary or on its immediate left depending on whether the shock or rarefaction is left-going or right-going respectively. Notice, therefore, that most of the information associated with the Riemann problem is indeed discarded. It is never used in the numerical scheme. This is a very useful insight that has led to the development of several inexpensive, yet very useful, Riemann solvers. When the zone is straddled by a rarefaction fan, we have to solve for the inner structure of the rarefaction.

Since solving for the structure of the rarefaction fan might be computationally expensive, especially when the problem becomes more complicated, we wonder whether we might be able to get by with using a rarefaction shock in its place? If we could get by with this choice, it would considerably simplify our design of Riemann solvers. This might seem like an acceptable simplification because a rarefaction shock would either be left or right-going and then we would only need to pick out the value of the solution to the right or left of the zone boundary. The simplification would be well-justified if the resulting numerical scheme continues to produce physical solutions.

To examine the adverse effects of rarefaction shocks, we study the solution of Burgers equation with the initial conditions given by $u_0(x) = -0.5$ for $x < 0$ and $u_0(x) = 1$ for $x \geq 0$. The crosses in Fig. 4.11a show the solution evaluated at a time of 0.35 with a first order accurate Godunov scheme in which all the rarefaction fans that straddle zone boundaries have been replaced by rarefaction shocks. The crosses in Fig. 4.11b show the solution at the same time with a first order accurate Godunov scheme where all the rarefaction fans that straddle a zone boundary have been treated correctly. The solid line in both Figs. 4.11a and 4.11b was produced by using a second order accurate scheme with the physically consistent Riemann solver being used at each zone boundary. We see from Fig. 4.11a that an unphysical rarefaction shock has developed in the first order solution. The rarefaction shock has -0.5 and 0.5 as its left and right states and these are just the values for which eqn. (4.10) would yield a non-propagating rarefaction shock. We can easily verify that the left and right values of the solution at the rarefaction shock violate Lax's entropy condition. The numerical solution has, therefore, produced a result that reflects the rarefaction shock in the underlying Riemann solver. Thus the consequence of using a Riemann solver that relies exclusively on rarefaction shocks is that the solution also develops an unphysical rarefaction shock. We therefore obtain the very important insight that the use of rarefaction shocks in our Riemann solver represents an unacceptable level of simplification. To obtain entropy-satisfying numerical solutions the numerical scheme has to be based on a Riemann solver that shows some recognition of the fact that rarefaction fans open up. The fix that is introduced into a Riemann solver to enable it to recognize the presence of a rarefaction fan that straddles a

zone boundary is called the *entropy fix*. It turns out that any reasonable entropy fix will usually work. However it is important to have an entropy fix in the Riemann solver if unphysical rarefaction shocks are to be avoided in the numerical solution.

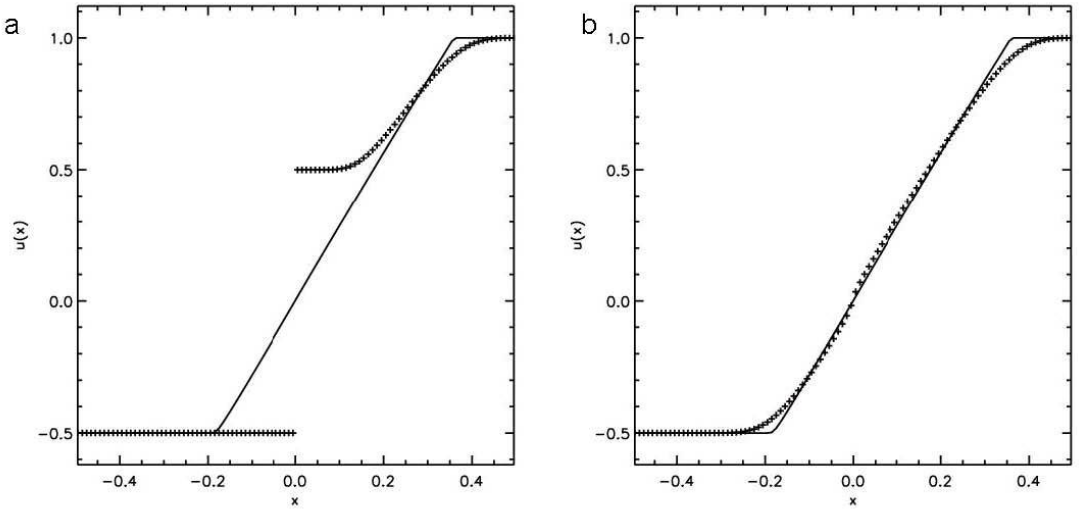

Figs. 4.11a and 4.11b show the importance of the entropy fix. The crosses in Fig. 4.11a shows the solution from a Godunov scheme when the Riemann solver permitted the formation of rarefaction shocks without introducting any correction for their existence. Fig. 4.11b shows the solution from a Godunov scheme when the Riemann solver used an entropy satisfying treatment of rarefaction fans. The solid line shows the solution from a second order TVD scheme with an exact Riemann solver and shows the physically consistent formation of the rarefaction fan.

If our only task were to numerically solve the Burgers equation, it would be easy enough to resort to an exact solution of the Riemann problem at each zone boundary. However, the solution of the exact Riemann problem can become progressively harder as the conservation law becomes more complicated. This is especially true when we are dealing with a system of conservation laws with a large number of components in the solution vector. Besides, as we have seen, much of the information that is produced by a Riemann solver is ignored when constructing a numerical flux. Our focus as computational scientists is entirely on the construction of the numerical flux. For that reason, several *approximate Riemann solvers* have been invented. Such approximate Riemann solvers attempt to retain only the essential elements of the Riemann problem while discarding those details that don't change the solution. We will see examples of

such approximate Riemann solvers in the next sub-section as well as in the next couple of chapters. The discussion in the above paragraph advises us that all such approximate Riemann solvers should indeed include an entropy fix for rarefaction fans.

4.5.2) Approximate Riemann Solvers – The HLL and LLF Riemann Solvers

While the previous sub-section has illustrated the importance of the entropy fix, we are still interested in formulating an approximate Riemann solver that produces an acceptably good result for the least amount of computation. Our experience has shown that the Riemann problem is a self-similar solution of the hyperbolic conservation law. Moreover, waves flow away from the initial discontinuity in the solution that gave rise to the Riemann problem. In designing an approximate Riemann solver, we wish to approximate the Riemann problem with the simplest self-similar *wave model* that will work successfully. A wave model is, therefore, a simpler proxy for the waves that emanate from an actual Riemann problem. It may not have all the information that is present in an actual Riemann problem, but the information is sufficient to yield physically consistent results in actual computations. It is purely an expedient for obtaining a good numerical flux in the most efficient way possible.

The solution of the internal structure of a rarefaction fan may still seem like an unnecessary level of detail and we will try to find ways to avoid it. The initial values of "u" to the left and right of the approximate Riemann problem are given by u_L and u_R. We see that when rarefactions that straddle a zone boundary are present, the fastest leftward propagating wave in the Riemann problem propagates with a speed $S_L = f'(u_L)$ where $S_L < 0$. Likewise, the fastest rightward propagating wave propagates with a speed $S_R = f'(u_R)$ where $S_R > 0$. These speeds are usually easy to find without solving for the detailed internal structure of the Riemann problem. For hyperbolic equations with convex fluxes we will show that the speeds S_L and S_R can always be found without solving the entire Riemann problem. We, therefore, approximate the Riemann problem as shown in Fig. 4.12. Fig. 4.12 shows the wave model for our approximate Riemann solver with the

extremal left- and right-propagating waves and with a constant state $\overline{u}^{(RS)}$ inserted between them. Fig. 4.12 follows the evolution of this approximate Riemann problem in a self-similar fashion for a time "T". In the spirit of an approximate Riemann solver, $\overline{u}^{(RS)}$ is then interpreted to be the resolved state associated with the Riemann problem. To fully appreciate the nature of the approximation, recall that Fig. 4.11b shows a rarefaction fan that originated from a Riemann problem at the origin. We saw in Sub-section 4.4.1 that the interior structure of an actual rarefaction fan depends on the details of the flux function. The rarefaction fan in Fig. 4.11b has evolved in a self-similar fashion to straddle the origin, quite like the wave model shown in Fig. 4.12. However, the actual rarefaction fan does not have a constant state between the bounding characteristics; the wave model shown in Fig. 4.12 does have a constant state between the bounding characteristics. As a result, our choice of a constant state $\overline{u}^{(RS)}$ really is an approximation stemming from our choice of a wave model.

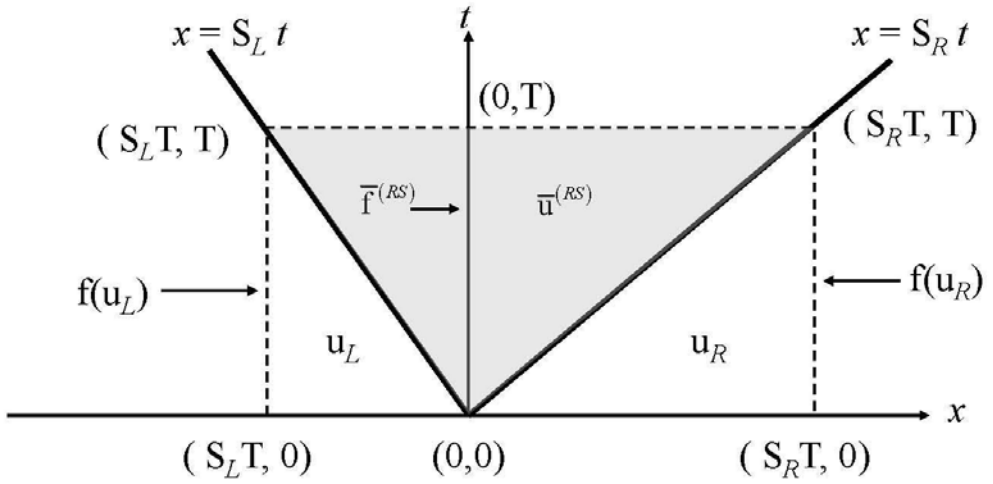

Fig. 4.12 shows an an approximate Riemann problem with right and left states given by u_R and u_L respectively. The extremal right and left-propagating waves are also shown by the thick lines in the figure. The resolved state and flux are given by $\overline{u}^{(RS)}$ and $\overline{f}^{(RS)}$ respectively.

To evaluate the details of our approximate Riemann solver, we need to find $\overline{u}^{(RS)}$. To do that, we integrate the conservation law from eqn. (4.1) in a weak sense over the rectangle formed by $(S_L T, 0)$, $(S_R T, 0)$, $(S_R T, T)$ and $(S_L T, T)$ in Fig. 4.12. Our derivation of simple waves in Sub-section 3.4.2 has already shown us how such an integration is to be carried out; see eqn. (3.32). The result is

$$\overline{u}^{(RS)} \left(S_R - S_L\right) T - u_R S_R T + u_L S_L T + f\left(u_R\right) T - f\left(u_L\right) T = 0 \tag{4.14}$$

The previous equation enables us to obtain the resolved state $\overline{u}^{(RS)}$ as

$$\overline{u}^{(RS)} = \frac{S_R u_R - S_L u_L - \left(f\left(u_R\right) - f\left(u_L\right)\right)}{\left(S_R - S_L\right)} \tag{4.15}$$

In order to use this approximate Riemann solver in a numerical scheme, we are actually interested in obtaining the resolved flux $\overline{f}^{(RS)}$. Notice that the resolved flux coincides with the time axis in Fig. 4.12, so we should pick a space-time domain that includes the time axis as one of its boundaries. This is obtained by integrating the conservation law from eqn. (4.1) in a weak sense over the rectangle formed by $\left(0, 0\right)$, $\left(S_R T, 0\right)$, $\left(S_R T, T\right)$ and $\left(0, T\right)$ in Fig. 4.12. The result is

$$\overline{u}^{(RS)} S_R T - u_R S_R T + f\left(u_R\right) T - \overline{f}^{(RS)} T = 0 \tag{4.16}$$

On substituting the expression for $\overline{u}^{(RS)}$ from eqn. (4.15), the above equation enables us to obtain the resolved flux $\overline{f}^{(RS)}$ as

$$\overline{f}^{(RS)} = \left[\frac{S_R}{S_R - S_L}\right] f\left(u_L\right) - \left[\frac{S_L}{S_R - S_L}\right] f\left(u_R\right) + \left[\frac{S_R S_L}{S_R - S_L}\right]\left(u_R - u_L\right) \tag{4.17}$$

This form of flux was first derived by Harten, Lax and van Leer (1983) and is usually referred to as the *HLL Riemann solver*. The HLL Riemann solver is an approximate Riemann solver because it does not solve the Riemann problem exactly. It is, however, a very popular Riemann solver and is easily extended to systems of hyperbolic equations. It is very easy to implement in numerical codes. It is also computationally inexpensive and gives reasonably good results for a large range of hyperbolic conservation laws. The

reader is advised to have an HLL Riemann solver as one of the options in her or his code and to resort to it when other Riemann solvers yield perplexing results. The HLL Riemann solver forms the basis for several successful CFD codes for astrophysics, space science and aeronautical and mechanical engineering.

Because we have not provided a complete method for obtaining S_L and S_R in all circumstances, our description of the HLL Riemann solver is still incomplete. For rarefaction waves that are known to straddle the zone boundary, i.e. when we have $f'(u_L) < 0$ and $f'(u_R) > 0$, we can indeed take the fastest left and right-propagating wave speeds to be $S_L = f'(u_L)$ and $S_R = f'(u_R)$. On the other hand, consider the right-going shock in Fig. 4.4e. We see that the largest rightward speed S_R for the right state is not $f'(u_R)$ but rather the shock speed "*s*" given by using eqn. (4.10). Similarly, if we had a leftward propagating shock in the problem, we would choose the smaller of $f'(u_L)$ and "*s*" , where "*s*" is given by using eqn. (4.10), in order to get S_L. Furthermore, in situations where we have an isolated right-going shock or rarefaction fan, we would like to have $\overline{f}^{(RS)} = f(u_L)$. Similarly, if we have an isolated left-going shock or rarefaction fan, we would like to have $\overline{f}^{(RS)} = f(u_R)$. All of these goals are achieved by the following elegant choice:

$$S_L = \min\left(f'(u_L),\, s,\, 0\right) \qquad S_R = \max\left(f'(u_R),\, s,\, 0\right) \tag{4.18}$$

Notice that when $f'(u_L)$, s and $f'(u_R)$ are all simultaneously positive definite, eqn. (4.18) gives us $S_L = 0$ and so we get $\overline{f}^{(RS)} = f(u_L)$ from eqn. (4.17). Similarly, when $f'(u_L)$, s and $f'(u_R)$ are all simultaneously negative definite, we have $S_R = 0$ so that eqn. (4.17) gives us $\overline{f}^{(RS)} = f(u_R)$. I.e. when either S_L or S_R is zero, the Riemann solver just gives us the upwinded fluxes, which are indeed stable. When $S_L < 0 < S_R$, we get contributions from all the three terms on the right hand side of eqn. (4.17). The first two

terms can be thought of as being a convex combination of the fluxes $f(u_L)$ and $f(u_R)$. The last term in eqn. (4.17) is proportional to $(u_R - u_L)$ and is, therefore, a diffusion term. This is how the HLL Riemann solver generates numerical viscosity in the presence of rarefaction fans. The numerical viscosity, which is proportional to the jump $(u_R - u_L)$, then causes the initial discontinuity to become smoothed out on the mesh. Larger jumps produce greater numerical viscosity and, therefore, stronger smoothing. This smoothing out of the solution enables the different characteristics (with their different propagation speeds) to emerge from the rarefaction fan. Without the presence of this numerical viscosity we would get rarefaction shocks, as seen in the previous sub-section. Notice that this viscosity is generated selectively only in regions where it is needed. In other words, compare eqn. (4.18) to eqn. (2.41) for the Lax-Friedrichs flux to observe that the latter flux always introduces viscosity regardless of whether it is warranted, whereas the flux in eqn. (4.18) only introduces viscosity at rarefaction fans that straddle the zone boundary.

While the discussion in the previous paragraph is strictly applicable to scalar, hyperbolic conservation laws with convex fluxes, we will see in Chapter 6 that it can be easily extended to systems of conservation laws. Taking our prototype Euler system as an example, when all the waves are propagating to the right or to the left we have a supersonic situation. As a result, situations where we have $S_R \geq S_L \geq 0$ or $S_L \leq S_R \leq 0$ in our Riemann solver are called *supersonic*. The name is applied even when the Riemann solver is not being used to solve the Euler equations. When some of the waves are left-propagating and the rest are right-propagating in the Euler system, the situation is referred to as subsonic. Consequently, situations where we have $S_L < 0 < S_R$ are referred to as *subsonic*, even when the Riemann solver is not being used to solve the Euler equations.

Just as we showed the consistency of the numerical flux function for linear hyperbolic systems in Sub-section 3.4.3, we can now demonstrate the same for our HLL flux in eqn. (4.17). Thus observe that as $u_L \to \bar{u}$ and $u_R \to \bar{u}$ for some constant state $\bar{u}$,

we can show that $\overline{f}^{(RS)} \to f(\overline{u})$. We have also seen that the numerical flux for a linear hyperbolic system should be properly upwinded. Demonstrating that the HLL flux is properly upwinded in the supersonic cases is easy, just evaluate eqn. (4.18) in the supersonic limits and examine the resulting fluxes from eqn. (4.17). The same property can be demonstrated for our HLL flux in the subsonic case by splitting it into the sum of two fluxes $f^+(u_L)$ and $f^-(u_R)$ as:

$$\overline{f}^{(RS)}(u_L, u_R) = f^+(u_L) + f^-(u_R) \quad \text{with}$$
$$f^+(u_L) \equiv \left[\frac{S_R}{S_R - S_L}\right]\left[f(u_L) - S_L u_L\right] \quad \text{and} \quad f^-(u_R) \equiv -\left[\frac{S_L}{S_R - S_L}\right]\left[f(u_R) - S_R u_R\right] \tag{4.19}$$

Then assuming the wave speeds S_L and S_R to be frozen, we can assert

$$\frac{\partial \overline{f}^{(RS)}(u_L, u_R)}{\partial u_L} = \frac{\partial f^+(u_L)}{\partial u_L} = \left[\frac{S_R}{S_R - S_L}\right]\left[f'(u_L) - S_L\right] \geq 0 \tag{4.20a}$$

$$\frac{\partial \overline{f}^{(RS)}(u_L, u_R)}{\partial u_R} = \frac{\partial f^-(u_R)}{\partial u_R} = -\left[\frac{S_L}{S_R - S_L}\right]\left[f'(u_R) - S_R\right] \leq 0 \tag{4.20b}$$

The inequality in eqn. (4.20a) prevails because $S_R \geq 0$ causes the first square bracket to be greater than or equal to zero, while $f'(u_L) \geq S_L$ causes the second square bracket to be greater than or equal to zero. The inequality in eqn. (4.20b) holds because $S_L \leq 0$ causes the first square bracket to be less than or equal to zero, while $f'(u_R) \leq S_R$ causes the second square bracket to be less than or equal to zero. Because $\partial f^+(u_L)/\partial u_L \geq 0$, we see that the flux $f^+(u_L)$ exclusively carries the contributions from right-going waves. Similarly, $\partial f^-(u_R)/\partial u_R \leq 0$ indicates that the flux $f^-(u_R)$ exclusively carries the contributions from the left-going waves. Even when the HLL Riemann solver is extended to systems of conservation laws, the flux vector for the system will be amenable to a similar splitting into parts that carry the contributions from right- and left-going waves.

As a result, eqn. (4.19) is a form of *flux vector splitting*. The flux vector splitting that we have achieved here is entirely a consequence of the wave model that we have adopted and demonstrates that the HLL flux is properly upwinded. Observe, however, that the $f^{+}(u_L)$ is not entirely independent of u_R, nor is $f^{-}(u_R)$ entirely independent of u_L for two important reasons. First, recall that freezing the wave speeds S_L and S_R , as we did above, was only an expedient to help us gain insight. Second, because the shock speed "*s*" in eqn. (3.18) couples the solutions on either side of a zone boundary, the split fluxes do depend on the contributions from the other side of the zone boundary.

Observe that the dissipation in the HLL Riemann solver is a consequence of the wave model that we adopted and increases as S_L becomes increasingly negative and S_R becomes increasingly positive. Eqns. (4.17) and (4.18), therefore, lend themselves to a further simplification. Let us say that we obtain an extremal value, S_{Max}, of the signal speed formed by taking the maximum of $|f'(u_L)|$, $|s|$ and $|f'(u_R)|$. By taking $S_R = S_{Max}$ and $S_L = -S_{Max}$ and using them in eqn. (4.17) we get

$$\overline{f}^{(RS)} = \frac{1}{2}\left(f(u_L) + f(u_R) - S_{Max}(u_R - u_L)\right) \quad \text{where} \quad S_{Max} \equiv \max\left(|f'(u_L)|, |s|, |f'(u_R)|\right) \tag{4.21}$$

This form of approximate Riemann solver was proposed by *Rusanov* (1961) though it is more often referred to as a *local Lax-Friedrichs Riemann solver* and is often called an LLF Riemann solver for short. Compare it to the Lax-Friedrichs flux in eqn. (2.41). The flux in eqn. (2.41) always introduces a substantial and often unwarranted amount of dissipation and the dissipation is proportional to the specifics of the mesh size and timestep, i.e. $\Delta x/\Delta t$, and not the solution. Eqn. (4.21) also contributes a certain amount of dissipation whenever it is used at a discontinuity. However, the amount of dissipation is scaled to the local wave speed in the flow and the size of the discontinuity. In other words, replacing $\Delta x/\Delta t$ in eqn. (2.41) by S_{Max}, yields eqn. (4.21). The amount of dissipation introduced by the LLF Riemann solver is in fact the largest amount of dissipation that would locally stabilize the flow. Eqn. (4.21) can then be viewed as an

improvement upon eqn. (2.41), which accounts for its name. Comparing eqns. (4.17) and (4.21) we see that there can be several situations where the HLL Riemann solver does not introduce any extra dissipation. On the other hand, the LLF Riemann solver always introduces some extra dissipation whenever it is invoked at a discontinuity. (If the discontinuity is a contact discontinuity in a CFD problem, such a dissipation would be entirely uncalled for. Thus a highly stabilizing Riemann solver can also be excessively dissipative in certain situations.) The LLF Riemann solver is, however, extremely easy to implement, easily extends to systems of conservation laws and carries a very low computational cost. Consequently, it is often used in several CFD codes. Because we have derived the LLF Riemann solver by relaxing the wave model in the HLL Riemann solver, the LLF Riemann solver inherits the properties of consistency and upwinding from its HLL progenitor.

Note that for fluid flow problems involving very strong shocks the LLF Riemann solver might indeed function well because of the surplus dissipation that it introduces. The penalty that one pays for using the LLF Riemann solver shows up when dealing with fluid flow problems with smooth solutions. In such problems, the surplus dissipation might diminish the quality of the solution. One should also use the LLF Riemann solver cautiously in fluid flow problems where a rarefaction might cavitate, i.e. produce a zero density and pressure in some part of the problem. The HLL Riemann solver does fine on such problems (Einfeldt *et al.* 1991) whereas the unduly excessive dissipation introduced by the LLF Riemann solver in such problems can have a negative effect.

Approximate Riemann Solvers for Non-Convex Fluxes

When the problem is non-convex, some aspects of the presentation provided here need to be modified. To appreciate the points of difference, let us consider the Buckley-Leverett problem that was presented at the end of Section 4.2. Consider the same initial conditions that we used in that box. They are $\mathrm{u}_0(x) = 1$ for $x < -0.4$ and $\mathrm{u}_0(x) = 0$ for $x \geq -0.4$ on the unit interval $[-0.5, 0.5]$. If these initial conditions were to be initialized

on a mesh and if the wave speed were calculated in each zone, we would come up with the result that the wave speed is exactly zero for all the zones in the mesh. This is because $f'(0)=0$ and $f'(1)=0$. One would naïvely assume that any timestep would be acceptable under these circumstances, but indeed that is not the case. This is because the solution assumes values between 0 and 1 as it evolves, and $f'(u)>0$ for $0<u<1$. Thus in order to find a good time step with which to evolve this problem numerically, we have to examine all values of the solution "u" in the range spanned by the initial conditions.

In other parts of this section, the convexity of the flux function had also given us some other advantages that we lose in the non-convex case. Observe eqn. (4.18). Notice that the extremal signal speeds can be obtained in the convex case by considering just the signal speeds at the left and right states of the Riemann problem and its shock propagation speed. However, S_L and S_R in eqn. (4.17) are interpreted as being the extremal values of the wave speed in the Riemann problem. For a non-convex flux we have to examine all the wave propagation speeds $f'(u)$ for all values of "u" in the range $[u_L, u_R]$ in order to derive S_L and S_R. The shock solution should also be included, as was done in eqn. (4.18), to obtain S_L and S_R. Consequently, the HLL Riemann solver can be used for treating non-convex problems. However, the interpretation of the extremal speeds has to be upgraded. Osher and Solomon (1982) and Osher (1984) have presented an implementable numerical strategy for solving the Riemann problem with a non-convex flux function, but the strategy also consists of examining/integrating the flux function for values of "u" that span the entire range $[u_L, u_R]$. From our example of the Buckley-Leverett problem we see that scanning the entire range is necessary if one wants to pick out the extremal wave speeds that one uses in a Riemann solver for a non-convex problem, however, it also increases the computational complexity of the Riemann solver.

Dumbser and Toro (2011) have achieved a significant simplification of the Riemann solver by Osher and Solomon (1982). Their approach consists of carrying out a three point numerical quadrature along a straight line in solution space that connects the

solution u_L to u_R . The method is reported to work very well even for systems of non-convex equations.

4.6) Boundary Conditions

In Section 3.5 we treated the boundary conditions for linear hyperbolic systems. All the insights gained there are equally applicable to non-linear, scalar conservation laws with one important point of difference. For linear hyperbolic systems, the wave speeds are entirely determined by the characteristic matrix and remain constant for all points in space and time. The presence of non-linearity in a scalar conservation law implies that the single wave speed is solution-dependent and can change from one location to the other as well as from one time to the next as the solution evolves. As a result, the boundary conditions may also have to adapt as the solution changes at the boundaries. This is illustrated in Fig. 4.13. Figs. 4.13a 4.13b and 4.13c show the space-time diagrams for the evolution of the characteristics in three different one-dimensional problems. The two vertical lines in each figure show the boundaries of the computational domain. The solid line in Fig. 4.13c shows the location of a shock. Fig. 4.13a shows us the evolution of a rarefaction fan on the mesh. We see that the left boundary should be treated as inflow and the right boundary should be treated as non-reflective outflow if the rarefaction fan is to be properly represented on the mesh. Fig. 4.13b shows a similar rarefaction fan except that this time both boundaries need to be treated as non-reflective outflow. Fig. 4.13c shows us the evolution of a shock as it eventually propagates off the right boundary of the computational domain. We see that before the shock hits the right boundary, both boundaries should be treated as inflow boundary conditions. After the shock hits the right boundary, the left boundary should be treated as inflow and the right boundary should be treated as non-reflective outflow. We see, therefore, that the boundary conditions need to adjust as the solution evolves. Moreover, as solution features flow off the mesh, the kinds of boundary conditions that are needed at a boundary may indeed change.

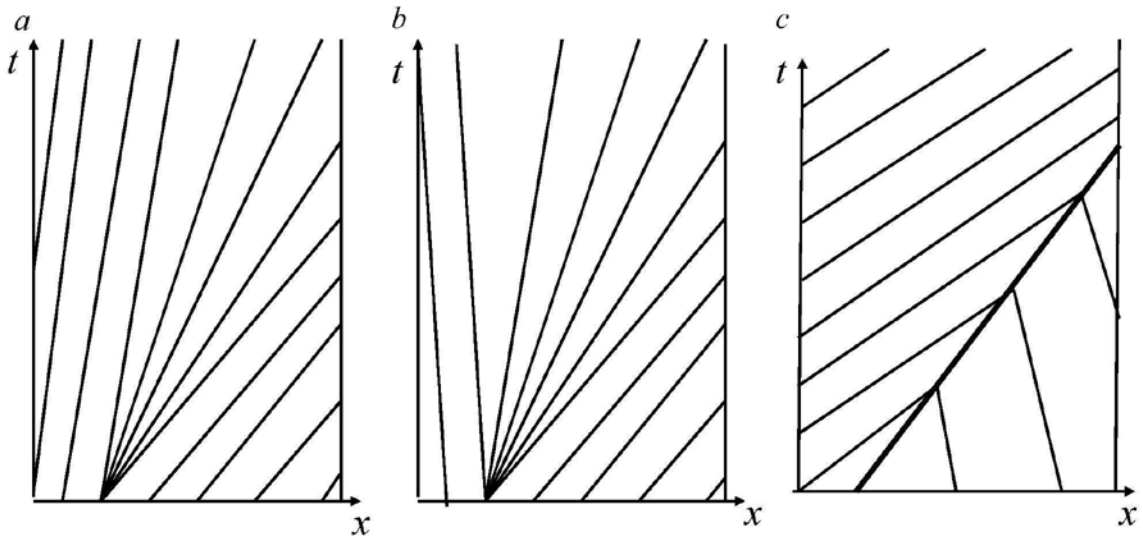

Figs. 4.13a 4.13b and 4.13c show the space-time diagrams for the evolution of the characteristics in three different one-dimensional problems. The two vertical lines in each figure show the boundaries of the computational domain. The solid line in Fig. 4.13c shows the location of a shock.

It is also worth observing that the variables that are initialized in the ghost zones may cause waves to propagate with signal speeds that can be larger than the signal speed that is represented in the interior of the computational domain. In such situations, which usually occur when a strong shock propagates in from a boundary, the timestep should be reduced to satisfy the CFL condition in the ghost zones. As a result, when dealing with non-linear hyperbolic problems the boundary conditions can also influence the timestep.

4.7) Numerical Methods

The numerical methods developed in Section 3.6 can all be extended to treat non-linear, scalar conservation laws. A *theorem by Lax and Wendroff* (1960) tells us that the problem should be discretized on a computational mesh using a consistent, stable and conservative method if weak solutions (i.e. shocks and rarefactions) are to be convergent as the mesh is refined. Besides, experience has shown non-conservative discretizations, even if they are stable, will cause shocks to propagate with the wrong speed. We therefore discretize the problem in conservation form. Since the Runge-Kutta and predictor-corrector schemes from that section are the ones that are routinely utilized, we

focus on those two here. The extension of the Lax-Wendroff scheme with limiters to treat non-linear, scalar conservation laws has been treated in Harten (1983a) and we do not repeat it here.

The two-stage Runge-Kutta scheme still relies on the update strategies that are catalogued in eqns. (3.50) or (3.51). For a scalar conservation law there is no need for a characteristic projection with the result that at each stage the limiter from eqn. (3.57) can be applied. The left and right states for the Riemann problem at each zone boundary can be obtained for each stage by using eqn. (3.55). The flux at each zone boundary can be obtained from eqn. (3.56). The HLL approximate Riemann solver can be used for obtaining a numerical flux with the correct amount of entropy enforcement. This completes our description of the two-stage Runge-Kutta scheme for non-linear, scalar conservation laws. We see, therefore, that the steps exactly parody those in Sub-section 3.6.2. The only major difference is that for a non-linear hyperbolic problem the boundary conditions that need to be used can change as the solution evolves on the computational mesh.

The predictor-corrector scheme also parodies the description in Sub-section 3.6.3. In each zone "*i*" we use the values in the neighboring zones to obtain a limited slope. Thus, in each zone "*i*" we have the zone-averaged value $\bar{u}_i^n$ as well as the undivided difference $\overline{\Delta u}_i^n$. Using eqns. (3.59) and (3.61) we obtain the time-centered left and right states at zone boundary "i+1/2" as

$$u_{L;i+1/2}^{n+1/2} = \bar{u}_i^n + \frac{1}{2}\,\overline{\Delta u}_i^n - \frac{1}{2}\,\frac{\Delta t}{\Delta x}\,f'\left(\bar{u}_i^n\right)\,\overline{\Delta u}_i^n \tag{4.22}$$

and

$$u_{R;i+1/2}^{n+1/2} = \bar{u}_{i+1}^n - \frac{1}{2}\,\overline{\Delta u}_{i+1}^n - \frac{1}{2}\,\frac{\Delta t}{\Delta x}\,f'\left(\bar{u}_{i+1}^n\right)\,\overline{\Delta u}_{i+1}^n \tag{4.23}$$

The time-centered left and right states from eqns. (4.22) and (4.23) can be used in an approximate HLL Riemann solver to obtain the fluxes at each zone-boundary. The final time-update follows from eqn. (3.63). This completes our description of the predictor-corrector scheme for scalar conservation laws.

The numerical methods described here indeed work very well and all the results shown in Figs. 4.4, 4.5, 4.6 and the figure in the box at the end of Section 4.2 were obtained by using these methods. The HLL Riemann solver was used to obtain all the results shown in those figures. For the non-convex case shown in the box at the end of Section 4.2, the extremal speeds for the Riemann solver were obtained by scanning all the intermediate states in the Riemann problem.

References

Chandrasekhar, S., *On the decay of plane shock waves*, Ballistic Research Laboratories, Report No. 423, Aberdeen Proving Ground, Maryland, (1943)

Dumbser M. and Toro E.F., *On universal Osher–type schemes for general nonlinear hyperbolic conservation laws*. Communications in Computational Physics, 10 (2011) 635–671

Einfeldt, B., Munz, C.-D., Roe, P.L. and Sjögreen, B, *On Godunov type methods near low densities*, Journal of Computational Physics, 92 (1991) 273-295

Harten, A., *High resolution schemes for conservation laws*, Journal of Computational Physics, 49 (1983a) 357-393

Harten, A, *On the symmetric form of conservation laws with entropy*, Journal of Computational Physics, 49 (1983b) 151-164

Harten, A. Lax, P.D. and van Leer, B, *On upstream differencing and Godunov-type schemes for hyperbolic conservation laws*, SIAM Review, 25 (1983) 289-315

Isaacson, E., Plohr, B. and Temple, B., *The Riemann problem near a hyperbolic singularity III*, SIAM Journal of Applied Mathematics, 48 (1988) 1302-1318

Isaacson, E. and Temple, B., *Analysis of a singular system of hyperbolic conservation laws*, J. Diff. Equations, 65 (1986) 250-268

Keyfitz, B., *A survey of nonstrictly hyperbolic conservation laws*, in Nonlinear Hyperbolic Problems, eds. C. Carasso, P.-A. Raviart and D. Serre, Lecture Notes in Mathematics 1270, Springer-Verlag (1986) 152-162

Keyfitz, B. and Mora, C.A., *Prototypes for nonstrict hyperbolicity in conservation laws*, Contemp. Math., 255 (2000) 125-137

Landau, L.D. & Lifshitz, E.M., "*Course of Theoretical Physics, volume 6: Fluid Mechanics*", (1987), Second Edition, Elsevier

Lax, P.D., *Hyperbolic Systems of Conservation Laws and the Mathematical Theory of Shock Waves*, SIAM Regional Conference in Applied Mathematics # 11 (1972)

Lax, P.D. and Wendroff, B., *Systems of conservation laws*, Communications in Pure and Applied Mathematics, 13 (1960) 217-237

LeFloch, P.G., *Hyperbolic Systems of Conservation Laws: The Theory of Classical and Non-classical Shock Waves*, Birkhauser (2002)

Oleinik, O., *Discontinuous solutions of non-linear differential equations*, Amer. Math. Soc. Transl. Ser. 2(26) (1957) 95-172

Oleinik, O., *Uniqueness and stability of the generalized solution of the Cauchy problem for a quasilinear equation*, Amer. Math. Soc. Transl. Ser., 2(33) (1964) 285-290

Osher, S., *Riemann solvers, the entropy condition and finite difference approximations*, SIAM Journal of Numerical Analysis, 21 (1984) 217-235

Osher, S. and Solomon, F., *Upwind difference schemes for hyperbolic systems of conservation laws*, Math. Comp., 38 (1982) 339-374

Rusanov, V.V., *Calculation of interaction of non-steady shock waves with obstacles*, J. Comput. Math. Phys. USSR, 1 (1961) 267

Schaeffer, D.G. & Shearer, M., *The classification of* 2×2 *systems of nonstrictly hyperbolic conservation laws, with application to oil recovery*, Communications in Pure and Applied Mathematics, 40 (1987a) 141-178

Schaeffer, D.G. & Shearer, M., *Riemann problems for nonstrictly hyperbolic* 2×2 *systems of conservation laws*, Trans. Amer. Math. Soc., 304 (1987b) 267-306

Problem Set

4.1) Show that eqn. (4.4) is indeed the solution to eqn. (4.2) with initial conditions $\mathrm{u}(x, t=0) = \mathrm{u}_0(x)$.

4.2) Derive the breaking time in eqn. (4.6).

4.3) Show that eqn. (4.8) is a solution of eqn. (4.7).

4.4) Show that eqn. (4.10) reduces to the speed $\frac{1}{2}\left(\mathrm{f}'(\mathrm{u}_R) + \mathrm{f}'(\mathrm{u}_L)\right)$ when u_R approaches u_L.

4.5) Consider the Burgers equation in non-conservative form $u_t + u\,u_x = 0$.

a) By multiplying the non-conservative form of Burgers equation with "2 u" show that it is also equivalent to the conservative form $\left(u^2\right)_t + \left(\frac{2}{3}u^3\right)_x = 0$.

b) Using eqn. (4.10), evaluate the shock speed for the initial conditions given by $u_0(x) = u_L = 2$ for $x < 0$ and $u_0(x) = u_R = 0$ for $x \geq 0$. Do this for Burgers equation in its standard, conservative form as well as in the conservative form obtained in this problem. Account for the difference and identify the point where we introduced a solipsism in this problem.

c) Would the numerical solution be the same if either of these two conservative forms are used to evolve a solution that is guaranteed to remain smooth for a certain span of time? I.e. we are only concerned with equality over the duration when the solution is smooth.

d) Would the numerical solution be the same if either of these two conservative forms are used to evolve a discontinuous solution?

4.6) Consider the solution of the Burgers equation with the initial conditions at $t = 0$ given by

$u_0(x) = 4$ for $x < -1$

$= 2$ for $-1 \leq x < 0$

$= 0$ for $x \geq 0$

a) Draw a space-time diagram for the characteristics and show the location of the shocks for $t < 1/2$. What happens at $t = 1/2$?

b) Draw the space-time diagram for the characteristics and show any shocks that might form for $t \geq 1/2$.

c) Now consider the initial conditions at $t = 0$ given by

$u_0(x) = 4$ for $x < -1/2$

$= 0$ for $x \geq -1/2$

Draw the space-time diagram for the characteristics and show the shock for all times $t \geq 0$.

d) If you could only examine the time evolution of each of these two problems for $t \geq 1/2$ then would you be able to retrieve the two different sets of initial conditions? What does that tell you about the time-reversibility of solutions that develop shocks? What can you say about the information being carried by the characteristics?

4.7) Consider the solution of the Burgers equation with the initial conditions given by $u_0(x) = 1$ for $-1 \leq x \leq 0$ and $u_0(x) = 2$ for all other points on the *x*-axis. Draw a space-time diagram for the characteristics. Find the point in space-time when the shock from $x = -1$ and the rarefaction fan emanating from the origin have their first interaction. Then obtain an ordinary differential equation for the evolution of the shock. Solve it numerically or analytically and plot out the locus of the shock on the space-time diagram.

4.8) Derive eqn. (4.15) from (4.14). Also derive (4.17) from (4.16).

Computer Exercises

4.1) This problem aims at reproducing the solution shown in Figs. 4.4a to 4.4d. Use the second order accurate Runge-Kutta timestepping strategy from Sub-Section 4.7 along with TVD limiting and the HLL Riemann solver to obtain the solution of the Burgers equation for this problem. Initialize the Gaussian shown in Fig. 4.4a on a mesh with a few hundred zones and obtain the results shown in Figs. 4.4b to 4.4d.

4.2) This problem aims at reproducing the shock solution shown in Figs. 4.5a to 4.5c as well as the rarefaction solution shown in Figs. 4.6a to 4.6c. Use the predictor corrector algorithm from Sub-Section 4.7 along with TVD limiting and the HLL Riemann solver to obtain the solution of the Burgers equation for this problem. Use a mesh with a hundred or so zones and study the effects of changing the mesh size for this problem. Initialize the shock shown in Fig. 4.5a and obtain the results in Figs. 4.5b and 4.5c. Then initialize the rarefaction shown in Fig. 4.6a and obtain the results in Figs. 4.6b and 4.6c.

4.3) Use the same algorithm and mesh that you developed in computer exercise 4.1. Solve the Buckley-Leverett problem with the initial conditions that coincide with the ones in the box at the end of 4.2. Notice that you have to modify the process of deducing the initial timestep. Also hold the CFL number down to 0.6 or less to make allowance for the fact that the signal speed inside the Riemann problem can be larger than the signal speeds of the left and right states. Because the problem is non-convex, the extremal speeds used in the approximate Riemann solver do not occur for the right and left states in the Riemann problem. You will need to make allowance for that.